(Received 6 February 2024, Accepted 10 May 2024, Scheduled 22 May 2024)

Negative Group Delay Prototype Filter Based on the Reciprocal Transfer Function of a Low-Pass Butterworth Filter Capped at Finite Out-of-Band Gain

Miodrag Kandic[*, 1, 2] and Greg E. Bridges[1, 3]

[1] *Department of Electrical and Computer Engineering, University of Manitoba, Winnipeg, Manitoba, Canada*
[2] *ORCID: 0000-0002-3673-4706*
[3] *ORCID: 0000-0001-8147-9882*

ABSTRACT: A Negative Group Delay (NGD) prototype filter design based on the reciprocal transfer function of a low-pass Butterworth filter of a given order, is presented. The out-of-band gain of the prototype transfer function is capped at a finite constant value via multiplication by a transfer function of a low-pass Butterworth filter with 3 dB bandwidth that is wider than the reciprocal function bandwidth. Such synthesized transfer function exhibits maximal magnitude characteristic flatness within the 3 dB bandwidth (Butterworth-like property), while it also exhibits NGD and satisfies Kramers-Kronig relations (causal transfer function). The prototype design achieves an NGD-bandwidth product that in the upper asymptotic limit as the design order increases, is a linear function of out-of-band gain in decibels. This is an improvement compared with previously reported cascaded first-order and second-order designs, which have NGD-bandwidth functional dependency of out-of-band gain in decibels to the power of 1/2 and 3/4, respectively. It is shown that the transfer function of the corresponding design transformed to a non-zero center frequency can be exactly implemented with a Sallen-Key topology employing parallel resonators, or approximately implemented with an all-passive ladder topology. An in-band magnitude/phase distortion metric is applied to the prototype designs, evaluated for Gaussian and sinc pulse input waveforms, and compared with values obtained for a well-known commonly used medium. It is also shown that when the specified bandwidth corresponds to the entire bandwidth over which the group delay characteristic is negative, the magnitude characteristic variation approximately equals half the out-of-band gain value in decibels. Therefore, for any NGD design with large out-of-band gain (typically higher than 6 dB), using the entire bandwidth where group delay is negative can result in strong levels of distortion and should be checked for applied waveforms.

1. INTRODUCTION

Negative group delay (NGD) phenomenon is observed in media exhibiting anomalous dispersion within a finite frequency bandwidth, and it is manifested via pulse waveform reshaping where certain features of the pulse (such as peak) at the medium output are time-advanced (negatively delayed) compared to their corresponding temporal location at the input. This phenomenon does not violate causality, since the onset of the waveform, or "front", is always positively delayed by such medium and does not exceed luminal velocity, as discussed in [1–3]. In the frequency domain, NGD phenomenon is represented by a positive slope of the phase characteristic over a finite frequency band. In addition to NGD, other examples of abnormal wave propagation phenomena include superluminal [4], backward wave propagation (negative refractive index) [5], and simultaneous negative phase and group velocity [6].

The work in [7] presents a proof showing that within a frequency band of abnormal propagation (such as NGD propagation), the magnitude response of a causal medium has a minimum, i.e., has an out-of-band gain, or equivalently the center frequency has maximum signal attenuation (SA) for gain-uncompensated designs. This is a direct consequence of Kramers-Kronig relations, which define magnitude and phase characteristic dependency in causal media. The out-of-band gain causes undesired amplification of transients associated with the propagation of pulses of finite duration, which have defined "turn on/off" points in time [8–11]. Such a transient response will follow any points of discontinuity in the waveform or any of its derivatives, not just the "turn on/off" times [12]. The out-of-band gain is proportional to the medium's transient amplitude response, and therefore, it is an undesired trade-off quantity accompanying the NGD phenomenon, as discussed and quantified for selected media in [8–11]. For a distributed medium composed of cascaded identical 1^{st}-order circuits at baseband frequencies, or equivalently cascaded identical 2^{nd}-order single-tuned resonators at an upshifted frequency band, the upper asymptotic limit of the NGD-bandwidth product was shown to be proportional to the square root of the out-of-band gain given in decibels [8]. Similarly, for an engineered causal medium with a chosen flat in-band NGD characteristic (linear phase characteristic with a positive slope) and its magnitude characteristic obtained from such phase characteristic via Kramers-Kronig relations, the same square-root of the decibel out-of-band gain is derived for the upper asymptotic limit of the

* Corresponding author: Miodrag Kandic (Miodrag.Kandic@umanitoba.ca).

NGD-bandwidth product [9], just with a higher proportional factor compared to [8]. For cascaded identical second-order circuits at baseband frequencies, the NGD-bandwidth product was shown to be proportional to the out-of-band gain given in decibels raised to the power of 3/4 [10].

In this paper, as an extension of the work in [8, 9] with cascaded 1^{st}-order, and in [10] with cascaded 2^{nd}-order rational functions, an NGD filter characterized by an N^{th}-order rational transfer function at baseband frequencies is presented. The proposed design is based on a reciprocal-Butterworth low-pass transfer function, where its out-of-band gain is capped at a finite constant value by a cascaded low-pass Butterworth filter transfer function with the same order and a wider bandwidth. This capping of the out-of-band gain makes the design feasible. It is shown that the transfer function of the corresponding design upshifted to a non-zero center frequency, i.e., a Band-Stop Filter (BSF) design with finite attenuation, can be exactly implemented with a Sallen-Key topology employing parallel resonators, or approximately implemented with an all-passive ladder topology with series and parallel resonators. The prototype design achieves an NGD-bandwidth product that in the upper asymptotic limit as the design order approaches infinity is a linear function of out-of-band gain in decibels, which is an improvement compared to the power of 1/2 relationship for designs presented in [8, 9] and the power of 3/4 for designs presented in [10].

An in-band magnitude/phase distortion metric based on the approach in [13, 14] and modified as in [10] is applied to the proposed design and for selected time-domain input waveforms. It is shown that if the distortion metric is to be kept below a prescribed acceptable value, the bandwidth used for waveform propagation must be reduced below the 3 dB cutoff in some cases. Many NGD designs in the literature report the entire bandwidth where the group delay is negative (typically larger than 3 dB bandwidth), and the usefulness of such bandwidth should be qualified since it may result in strong levels of distortion of propagated waveforms. Different NGD circuit designs, such as those reported in [8, 15–31], are commonly compared for their achieved NGD-bandwidth product and the associated trade-off quantity out-of-band gain (signal attenuation for gain-uncompensated designs). Additionally, it would be beneficial to check and compare such NGD designs for the in-band magnitude/phase distortion discussed in this paper.

2. PROTOTYPE NGD FILTER BASED ON CAPPED RECIPROCAL LOW PASS BUTTERWORTH FILTER TRANSFER FUNCTION

NGD designs reported in [8, 9] are based on a 1^{st}-order rational transfer function at baseband frequencies, which, when being upshifted to a higher center frequency, yields a 2^{nd}-order rational transfer function tuned at that center frequency. Similarly, the design reported in [10] is based on a 2^{nd}-order rational transfer function at baseband frequencies, with complex poles and zeros, so it cannot be factorized into the type of 1^{st}-order functions reported in [8, 9]. When such 2^{nd}-order baseband transfer function is upshifted to a higher center frequency, it yields a product of two 2^{nd}-order rational transfer functions (overall 4^{th}-order) tuned at two different frequencies such that the center frequency is a geometric mean of the two tuned frequencies [10].

The extension of the above approach to baseband designs composed of 3^{rd}, 4^{th}, or higher orders of rational transfer functions, which cannot be factorized into identical 1^{st} and/or 2^{nd}-order transfer functions, is not straightforward. A different approach to formulate such described NGD-exhibiting rational transfer function of any order is proposed here, based on a ratio of two low-pass Butterworth filter transfer functions of the same order, but with different bandwidths, and given by:

$$\begin{aligned} H(j\omega) &= H_{\text{reciprocal-LP}}(j\omega) \cdot H_{\text{capping-LP}}(j\omega) \\ &= \frac{1}{H_{N^{th}\text{-LP-Buttw}}\left(j\frac{\omega}{\omega_{c1}}\right)} \\ &\quad \cdot H_{N^{th}\text{-LP-Buttw}}\left(j\frac{\omega}{\omega_{c2}}\right). \end{aligned} \tag{1}$$

For NGD to exist around the center frequency, the 3 dB cut-off frequency of the capping function needs to be larger than that of the reciprocal function, $\omega_{c2} > \omega_{c1}$. The different bandwidths of the reciprocal and capping functions also ensure that poles and zeros of the overall transfer function are different. The novel design process is detailed in a patent application [32]. A magnitude plot of a transfer function (1) example is illustrated in Fig. 1, showing a finite out-of-band gain, A. The example shows a gain-compensated design, but it can also be scaled to represent a passive design (magnitude below 0 dB) without affecting the group delay characteristic.

The overall capped reciprocal-Butterworth low-pass transfer function design shown in Fig. 1 satisfies the requirement that an NGD transfer function magnitude has a minimum within the in-band region around the center frequency [7]. A transfer function having similar attributes was described by Ravelo [33], exhibiting both NGD and finite out-of-band gain, for the 1^{st}-order baseband and 2^{nd}-order bandpass cases.

The core term of the proposed design, which produces the NGD in (1), is a reciprocal function of a Butterworth low pass filter transfer function, $H_{Nth-LP-Buttw}(j\omega/\omega_{c1})$, with a 3 dB cut-off frequency ω_{c1} (which is also approximately the 3 dB cut-off frequency of the overall transfer function). This reciprocal function term alone would result in an infinite out-of-band gain, or in its gain-uncompensated scaled version with 0 dB gain maximum at out-of-band frequencies, it would result in an infinite attenuation at the center frequency. Therefore, to make the design practical and feasible, a "capping" of the out-of-band gain is also needed to limit it to a finite value. As given in (1), this can be achieved by multiplying the reciprocal transfer function with a low-pass Butterworth transfer function, $H_{Nth-LP-Buttw}(j\omega/\omega_{c2})$, with a larger 3 dB bandwidth, $\omega_{c2} > \omega_{c1}$. The capping function in (1) emerges as the denominator polynomial since it corresponds to the classical low-pass Butterworth filter. Therefore, the overall transfer function has poles in the $s = j\omega$ complex Left Half-Plane (LHP) and is inherently stable. The larger bandwidth of the multiplying

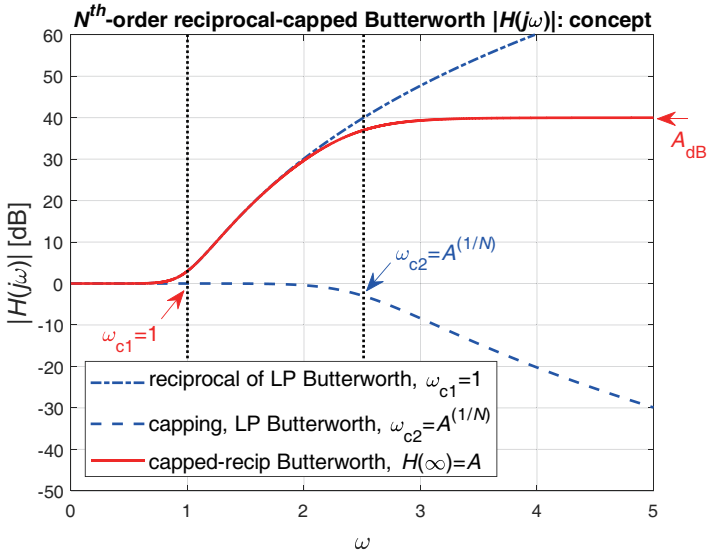

FIGURE 1. Example 5^{th}-order capped reciprocal-Butterworth NGD baseband design, $A = 100$ ($A_{\text{dB}} = 40$ dB), $N = 5$, $\omega_{c1} = 1$, $\omega_{c2} = A^{1/N} = 2.512$.

capping function ensures that the in-band part of the reciprocal function is not affected due to a near-flat magnitude response of a low-pass Butterworth filter transfer function for frequencies that are sufficiently below its cut-off frequency, ω_{c2}. Further, the capping function provides near-ideal cancellation of the positive out-of-band slope of the reciprocal function past frequency ω_{c2}, since both functions are of the same Butterworth filter type with the same order.

The proposed design transfer function expressions of baseband design order N are provided in (2a) and (2b) for even and odd values, respectively:

$$H_{N-even}(j\omega) = \prod_{k=1}^{N/2}\left(\frac{\omega^2 - jg_k\omega - 1}{\left(\frac{\omega}{A^{1/N}}\right)^2 - jg_k\frac{\omega}{A^{1/N}} - 1}\right) = A\prod_{k=1}^{N/2}\left(\frac{\omega^2 - jg_k\omega - 1}{\omega^2 - jg_kA^{1/N}\omega - A^{2/N}}\right), \quad (2a)$$

$$H_{N-odd}(j\omega) = A\frac{\omega - j}{\omega - jA^{1/N}} \cdot \prod_{k=1}^{(N-1)/2}\left(\frac{\omega^2 - jg_k\omega - 1}{\omega^2 - jg_kA^{1/N}\omega - A^{2/N}}\right), \quad (2b)$$

where the factorized functions' parameter g_k is the same as in N^{th}-order Butterworth low-pass filter:

$$g_k = 2\cdot\sin\left(\frac{2k-1}{2N}\pi\right). \quad (2c)$$

It is evident that expressions (2a) and (2b) are normalized to the reciprocal function cut-off frequency, i.e., $\omega_{c1} = 1$, and that the capping function cut-off frequency is related to the out-of-band gain as $\omega_{c2}/\omega_{c1} = A^{1/N}$.

The proposed capped reciprocal-Butterworth filter transfer function design is different from the design reported in [25], where a Butterworth-like filter transfer function response (flat magnitude characteristic) is present in the out-of-band region, but not in the in-band region around the center frequency where NGD is exhibited. From expressions (2a)–(2c), transfer functions for the first five orders of the proposed design, and for given out-of-band gain A, are given by:

$$H_1(j\omega) = A\left(\frac{\omega - j}{\omega - jA}\right), \quad (3a)$$

$$H_2(j\omega) = A\frac{\omega^2 - j\sqrt{2}\omega - 1}{\omega^2 - j\sqrt{2}\sqrt{A}\omega - A}, \quad (3b)$$

$$H_3(j\omega) = A\left(\frac{\omega - j}{\omega - jA^{1/3}}\right)\cdot\left(\frac{\omega^2 - j\omega - 1}{\omega^2 - jA^{1/3}\omega - A^{2/3}}\right), \quad (3c)$$

$$H_4(j\omega) = A\left(\frac{\omega^2 - j2\sin\left(\frac{\pi}{8}\right)\omega - 1}{\omega^2 - j2\sin\left(\frac{\pi}{8}\right)A^{1/4}\omega - A^{2/4}}\right) \cdot\left(\frac{\omega^2 - j2\sin\left(\frac{3\pi}{8}\right)\omega - 1}{\omega^2 - j2\sin\left(\frac{3\pi}{8}\right)A^{1/4}\omega - A^{2/4}}\right), \quad (3d)$$

$$H_5(j\omega) = A\left(\frac{\omega - j}{\omega - jA^{1/5}}\right) \cdot\left(\frac{\omega^2 - j2\sin\left(\frac{\pi}{10}\right)\omega - 1}{\omega^2 - j2\sin\left(\frac{\pi}{10}\right)A^{1/5}\omega - A^{2/5}}\right) \cdot\left(\frac{\omega^2 - j2\sin\left(\frac{3\pi}{10}\right)\omega - 1}{\omega^2 - j2\sin\left(\frac{3\pi}{10}\right)A^{1/5}\omega - A^{2/5}}\right). \quad (3e)$$

It can be noted that 1^{st}-order design transfer function (3a) corresponds to the design reported in [8, 9], whereas (3b) corresponds to the 2^{nd}-order design reported in [10]. These previously reported 1^{st} and 2^{nd}-order designs were formulated via

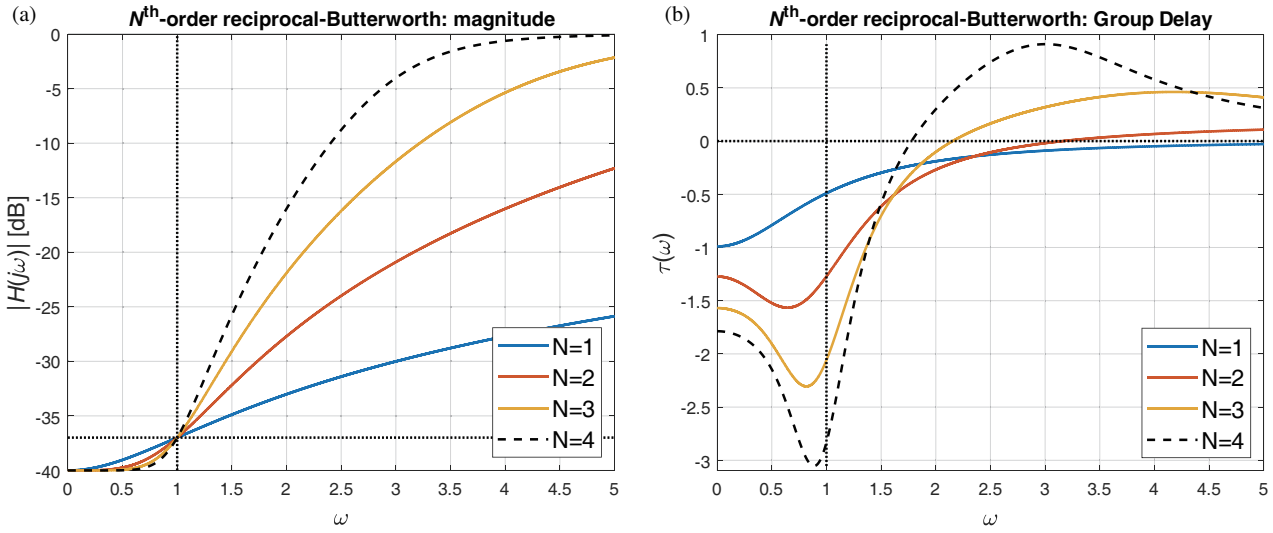

FIGURE 2. Proposed baseband transfer function NGD design with out-of-band gain $A = 100$ (40 dB) and $N = 1, 2, 3, 4$ order, (a) magnitude and (b) group delay.

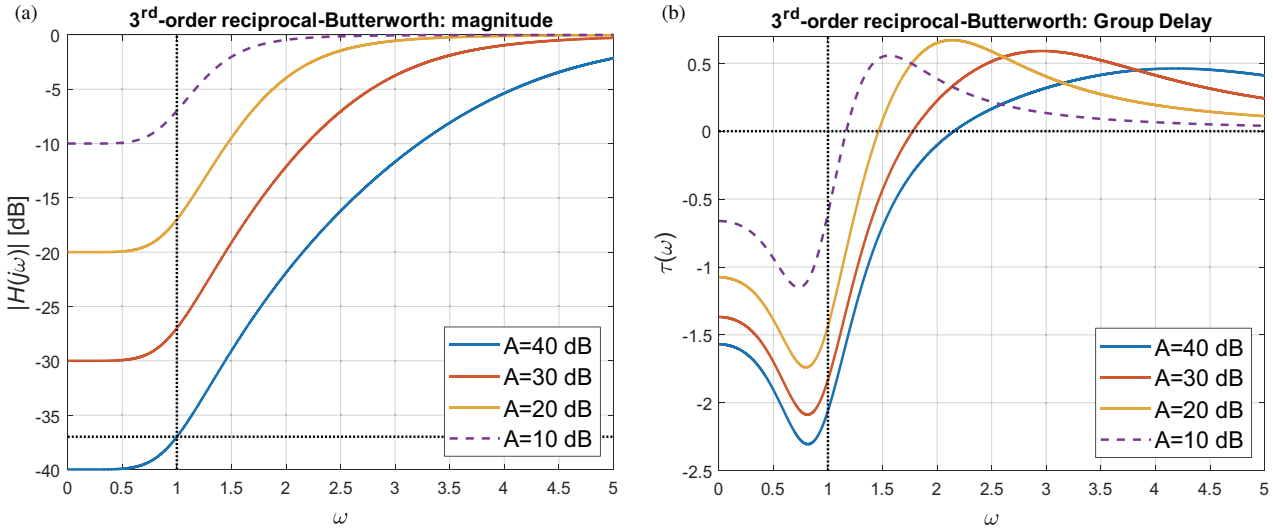

FIGURE 3. Proposed baseband transfer function NGD design of $N = 3^{rd}$-order and with out-of-band gains $A = 10$ dB, 20 dB, 30 dB, 40 dB, (a) magnitude and (b) group delay plots.

approaches different from the one presented here but yielded the same transfer functions. Further, the 2^{nd}-order approach reported in [10] would prove challenging to extend to higher orders, whereas the approach presented here yields explicit expressions (2a)–(2c) that can be easily applied to any order.

Expressions (2a)–(2b) and correspondingly (3a)–(3e) can also be divided by the out-of-band gain A, to represent their scaled ($-A_{\text{dB}}$ offset on dB magnitude plot), gain-uncompensated versions with center frequency magnitude attenuation $1/A$ ($-A_{\text{dB}}$), and their out-of-band magnitude characteristic always less than 1 (below 0 dB). Magnitude plots are shown in Fig. 2(a) for several different design orders, and in Fig. 3(a) for several different out-of-band gains (relative to center frequency attenuations). Corresponding group delay plots are shown in Figs. 2(b) and 3(b), which are the same for gain-uncompensated (center frequency attenuation $1/A$) and gain-compensated scaled versions (center frequency transfer function magnitude of 1, or 0 dB) of the transfer functions.

From Fig. 2(b), for designs of order $N > 1$ it is noted that as frequency increases from the center frequency, the group delay characteristic has a negative slope at first before a slope reversal close to the 3 dB band edge. In contrast, the 1^{st}-order design group delay characteristic has a minimum at the center frequency, and it monotonically increases to the 3 dB band edge.

A general form of the 1^{st}-order factorized rational functions appearing in the proposed baseband design odd-order transfer functions (2b), their corresponding phase and group delay characteristics, and their center frequency NGD are, respectively, given by:

$$H_{1st}(j\omega) = \frac{\omega - j\Delta\omega_1}{\omega - j\Delta\omega_2}, \tag{4a}$$

$$\varphi_{1st}(\omega) = \tan^{-1}\left(\frac{-\Delta\omega_1}{\omega}\right) - \tan^{-1}\left(\frac{-\Delta\omega_2}{\omega}\right), \quad (4b)$$

$$\tau_{1st}(\omega) = -\frac{d\varphi_{1st}(\omega)}{d\omega} = -\frac{\Delta\omega_1}{\omega^2+\Delta\omega_1^2} + \frac{\Delta\omega_2}{\omega^2+\Delta\omega_2^2}, \quad (4c)$$

$$\tau_{1st}(0) = -\frac{1}{\Delta\omega_1} + \frac{1}{\Delta\omega_2} = -\left(1 - \frac{1}{A^{1/N}}\right). \quad (4d)$$

Similarly, a general form of the 2^{nd}-order factorized rational functions appearing in the proposed baseband design transfer functions (2a) and (2b) for any order $N \geq 2$, their corresponding phase and group delay characteristics, and their center frequency NGD are, respectively, given by:

$$H_{2nd}(j\omega) = \frac{\omega^2 - j\Delta\omega_1\omega - \omega_{01}^2}{\omega^2 - j\Delta\omega_2\omega - \omega_{02}^2}, \quad (5a)$$

$$\varphi_{2nd}(\omega) = \tan^{-1}\left(\frac{-\Delta\omega_1\omega}{\omega^2 - \omega_{01}^2}\right) - \tan^{-1}\left(\frac{-\Delta\omega_2\omega}{\omega^2 - \omega_{02}^2}\right), \quad (5b)$$

$$\begin{aligned}\tau_{2nd}(\omega) &= -\frac{d\varphi_{2nd}(\omega)}{d\omega} \\ &= \frac{-\Delta\omega_1\left(\omega^2+\omega_{01}^2\right)}{\left(\omega^2-\omega_{01}^2\right)^2 + \Delta\omega_1^2\omega^2} \\ &\quad + \frac{\Delta\omega_2\left(\omega^2+\omega_{02}^2\right)}{\left(\omega^2-\omega_{02}^2\right)^2 + \Delta\omega_2^2\omega^2}, \end{aligned} \quad (5c)$$

$$\tau_{2nd}(0) = -\frac{\Delta\omega_1}{\omega_{01}^2} + \frac{\Delta\omega_2}{\omega_{02}^2} = -g_k\left(1 - \frac{1}{A^{1/N}}\right) \quad (5d)$$

The numerators of the proposed design rational transfer functions (2a)–(2b), and therefore numerators of the example functions (3a)–(3e), correspond to the uncapped reciprocal low-pass Butterworth filter transfer functions resulting in their 3 dB cut-off frequency being exactly at the normalized base frequency, $\omega_{c1} = 1$. The denominators, however, which are needed for magnitude characteristic capping, effectively increase the overall transfer function 3 dB cut-off frequency above the normalized $\omega_{c1} = 1$ frequency. To correct this cut-off frequency drift, a frequency correction factor can be applied by replacing ω by $\omega/C_{\omega-3\,\text{dB}}$, in all $H(j\omega)$, $\phi(\omega)$, and $\tau(\omega)$ expressions presented so far, with the correction factor given by:

$$C_{\omega-3\,\text{dB}} = \left(1 - \frac{2}{A^2}\right)^{\frac{1}{2N}}. \quad (6)$$

For example, if $A = 100$ (40 dB) then the correction factor for order $N = 1$ yields $C_{\omega-3\,\text{dB}} = 0.9999$, and for higher orders even closer to 1.0, which renders the correction factor negligible for this relatively high value of out-of-band gain. A lower out-of-band gain of $A = 3.1623$ (10 dB) for example, yields $C_{\omega-3\,\text{dB}} = 0.8944$, 0.9457, 0.9635 for $N = 1$, 2, 3, respectively, and it needs to be considered.

In addition to replacing ω by $\omega/C_{\omega-3\,\text{dB}}$, group delay $\tau(\omega)$ expressions need to be divided by $C_{\omega-3\,\text{dB}}$ as well, since those are obtained as a derivative of the phase characteristic. With this in mind and considering that the products of 1^{st} and 2^{nd}-order factorized functions in (2a) and (2b) translate into a sum of group delay characteristics of those factorized functions given by (4c) and (5c), the 3 dB bandwidth corrected center frequency NGD values for even and odd orders are respectively given by:

$$\begin{aligned}\tau_{even}(0) &= -\frac{1}{C_{\omega-3\,\text{dB}}}\sum_{k=1}^{N/2} g_k\left[1 - \frac{1}{A^{1/N}}\right] \\ &= -\frac{2}{C_{\omega-3\,\text{dB}}}\left(1 - \frac{1}{A^{1/N}}\right)\sum_{k=1}^{N/2}\sin\left(\frac{2k-1}{2N}\pi\right), \end{aligned} \quad (7a)$$

$$\begin{aligned}\tau_{odd}(0) &= -\frac{1}{C_{\omega-3\,\text{dB}}}\left(1 - \frac{1}{A^{1/N}}\right) \\ &\quad \left[1 + 2\cdot\sum_{k=1}^{(N-1)/2}\sin\left(\frac{2k-1}{2N}\pi\right)\right]. \end{aligned} \quad (7b)$$

In Fig. (2b) examples with $A = 100$ (40 dB), expressions (7a) and (7b) yield center frequency NGD values, NGD $= -\tau(0) = 0.9901$ s, 1.2729 s, 1.5692 s, 1.7868 s for $N = 1$, 2, 3, 4, respectively. Keeping in mind that the 3 dB bandwidth corrected cut-off frequency is $\omega_{c1} = 1$, Fig. (2b) center frequency values yield NGD-bandwidth product values of NGD$\cdot\Delta f$ = NGD $\cdot\, \omega_{c1}/\pi = 0.3152$, 0.4052, 0.4995, 0.5688 for $N = 1$, 2, 3, 4, respectively. Similarly, Fig. (3b) values for 3^{rd}-order designs yield center frequency NGD values of 0.6616s, 1.0753 s, 1.3680 s, 1.5692 s or NGD-bandwidth product values of NGD$\cdot\Delta f = 0.2106$, 0.3423, 0.4354, 0.4995, for $A_{\text{dB}} = 10$ dB, 20 dB, 30 dB, 40 dB, respectively.

3. BASEBAND NGD FILTER TRANSLATION TO BAND-STOP-FILTER (BSF)

To shift an NGD-exhibiting baseband transfer function to its BSF equivalent (with a finite band-stop attenuation), centered at a non-zero center frequency ω_0, the same frequency transformation that transforms a low-pass filter to its bandpass equivalent is applied [10]:

$$\omega \to \frac{1}{2}\left(\omega - \frac{\omega_0^2}{\omega}\right), \quad (8)$$

where both ω and ω_0 are normalized to the baseband 3 dB cut-off frequency ω_{c1}. For the 2^{nd}-order baseband transfer function form that is a part of any odd or even N^{th}-order (given $N > 1$) reciprocal-Butterworth transfer function presented in this paper, given by expressions (2a), (2b), application of the frequency transformation given by expression (8) yields the following baseband/BSF pair of transfer functions:

$$H_{BB2}(j\omega) = \frac{\omega^2 - j\Delta\omega_1\omega - \omega_{01}^2}{\omega^2 - j\Delta\omega_2\omega - \omega_{02}^2}, \quad (9a)$$

$$H_{BSF2}(j\omega) = \left(\frac{\omega^2 - j\Delta\omega_{1p}\omega - \omega_{01p}^2}{\omega^2 - j\Delta\omega_{2p}\omega - \omega_{02p}^2}\right)\cdot\left(\frac{\omega^2 - j\Delta\omega_{3p}\omega - \omega_{03p}^2}{\omega^2 - j\Delta\omega_{4p}\omega - \omega_{04p}^2}\right). \quad (9b)$$

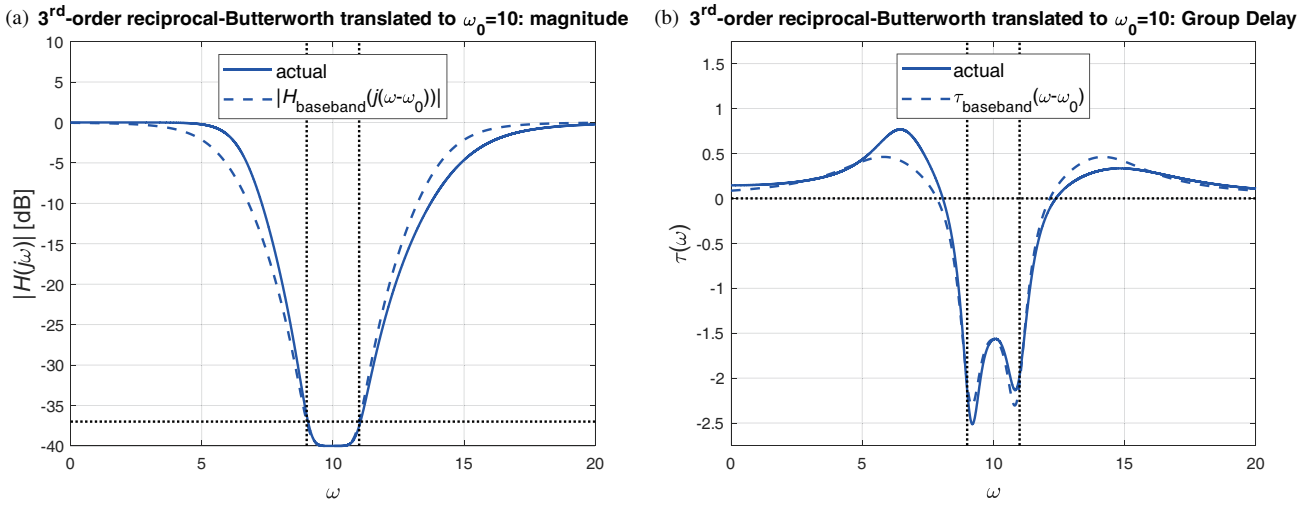

FIGURE 4. Example 3^{rd}-order proposed baseband transfer function (a) magnitude and (b) group delay responses translated to $\omega_0 = 10\omega_c = 10$ center frequency and compared with corresponding translated ideal baseband responses.

The eight frequency parameters in expression (9b) can be calculated from the four baseband parameters appearing in (9a), via explicit expressions reported in [10]. For referencing purposes in subsequent sections in this paper, a few selected relationships between parameters in (9b) are [10]:

$$\omega_{03p} = \frac{\omega_0^2}{\omega_{01p}}, \quad \Delta\omega_{3p} = \frac{\omega_0^2}{\omega_{01p}^2}\Delta\omega_{1p} = \frac{\omega_{03p}}{\omega_{01p}}\Delta\omega_{1p}. \tag{10}$$

From expressions (10) it is noted that the upshifted design center frequency ω_0 is a geometric mean of the two 2^{nd}-order rational transfer functions numerator's tuned frequencies, ω_{01p} and ω_{03p}. Further, the quality factors, or the tuned frequency to bandwidth ratios, are the same for the two functions numerators, $\omega_{01p}/\Delta\omega_{1p} = \omega_{03p}/\Delta\omega_{3p}$. A variation of expressions (10) applies to the corresponding denominator parameters, where indices 1 and 3 are replaced by 2 and 4, respectively.

For a 1^{st}-order NGD baseband transfer function that is a part of any odd N^{th}-order reciprocal-Butterworth transfer function presented in this paper, application of the frequency transformation given by expression (8) yields the following baseband/BSF pair of transfer functions:

$$H_{BB1}(j\omega) = \frac{\omega - j\Delta\omega_5}{\omega - j\Delta\omega_6}, \tag{11}$$

$$H_{BSF1}(j\omega) = \frac{\omega^2 - j\Delta\omega_{5p}\omega - \omega_0^2}{\omega^2 - j\Delta\omega_{6p}\omega - \omega_0^2}, \tag{12}$$

where $\Delta\omega_{5p} = 2\Delta\omega_5$ and $\Delta\omega_{6p} = 2\Delta\omega_6$. The transfer function given by (12) is of the same form reported in [8, 9]; however, in this paper it is only a part of the overall transfer function.

As an example, consider a 3^{rd}-order reciprocal-Butterworth baseband transfer function exhibiting NGD given by (3c), with out-of-band gain $A = 100$, or 40 dB (ω and all parameters are normalized to $\omega_c = 1$, with the 3 dB correction factor $C_{\omega-3\,\text{dB}} = (1 - 2/100^2)^{1/6} \approx 1.0$ in this case):

$$H_{BB3}(j\omega) = \frac{\omega - j}{\omega - j100^{1/3}}\left(\frac{\omega^2 - j\omega - 1}{\omega^2 - j100^{1/3}\omega - 100^{2/3}}\right). \tag{13}$$

Employing expression (8), after factorization the frequency upshift to $\omega_0 = 10\omega_c = 10$ chosen in this example, yields:

$$\begin{aligned} H_{BSF3}(j\omega) &= \frac{\omega^2 - j2\omega - 10^2}{\omega^2 - j9.2832\omega - 10^2} \\ &\cdot \left(\frac{\omega^2 - j1.0864\omega - 10.9064^2}{\omega^2 - j6.4081\omega - 14.9294^2}\right) \\ &\cdot \left(\frac{\omega^2 - j0.9136\omega - 9.1704^2}{\omega^2 - j2.875\omega - 6.6982^2}\right). \end{aligned} \tag{14}$$

The plot in Fig. 4 depicts magnitude and group delay characteristics of the transfer function (14), with overall out-of-band gain $A = 40$ dB and normalized bandwidth $\Delta\omega = 2\omega_c = 2$. A close in-band match is observed compared with the translated ideal baseband responses (expression (13) with $\omega \to \omega - \omega_0$). This transfer function achieves a center frequency NGD of 1.5692 s, or an NGD-bandwidth product of $\text{NGD} \cdot \Delta f = \text{NGD} \cdot \omega_c/\pi = 0.4995$ (the same as baseband one, as in Fig. 2(b).

Note that the factorized 2^{nd}-order baseband rational transfer function term from expression (13) yields two 2^{nd}-order terms when being translated to its non-zero center frequency equivalent (14). These have numerators with resonant frequencies (10.9064 and 9.1704) which differ from the corresponding denominators resonant frequencies (14.9294 and 6.6982). It is only the products of the resonant frequencies in the numerator and the denominator that are the same ($10.9064 \times 9.1704 = 14.9294 \times 6.6982 = \omega_0^2 = 100$), as noted from the geometric mean property in (10), and required in order to yield $H(0) = 1$ (out-of-band gain $H(\omega \to \infty)/H(\omega_0) = H(0)/H(\omega_0) = 1/(1/A) = A$). This difference in numerators' and denominators' resonant frequency values is the reason that the transfer

function (14) cannot be realized exactly via buffered passive resonators. However, a particular version of the Sallen-Key topology, presented next, has been found as able to achieve such a transfer function.

4. EXACT IMPLEMENTATION WITH SALLEN-KEY TOPOLOGY

A Sallen-Key topology with a cascaded resonator at the output, as depicted in Fig. 5 schematic, can achieve the 3^{rd}-order reciprocal-Butterworth baseband transfer function translated to higher center frequency ω_0, such as one given by expression (14). This design is similar to the well-known low-pass Sallen-Key design that has capacitors in place of R_F and R_G resistors in Fig. 5, and resistors in place of Z_1 and Z_2, and with no additional resonator after the output of the op-amp. Cascaded versions of the topology in Fig. 5 can achieve higher order reciprocal-Butterworth designs. The corresponding transfer function of the topology in Fig. 5 (V_{in} is assumed to be an ideal/buffered source, and V_{out} is assumed to be terminated in system impedance Z_0), and its input impedance (disregarding the optional input impedance matching resistor, R_m, which can be used with a non-ideal/non-buffered source) are given by, respectively:

$$H(j\omega) = \frac{V_{out}}{V_{in}} = \frac{R_G \cdot R_F}{R_G \cdot R_F + Z_1 \cdot Z_2 + R_F \cdot (Z_1 + Z_2)} \cdot \frac{Z_0}{Z_0 + Z_3}, \quad (15)$$

$$Z_{in} = \frac{R_G \cdot R_F + Z_1 \cdot Z_2 + R_F \cdot (Z_1 + Z_2)}{R_F + Z_2}. \quad (16)$$

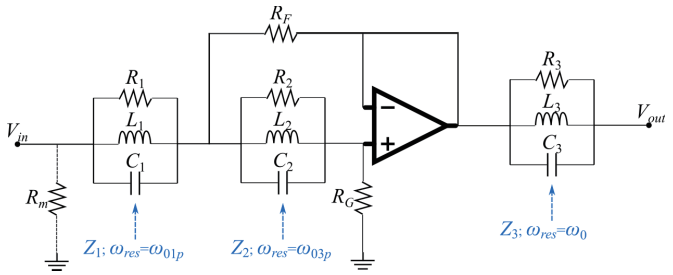

FIGURE 5. Sallen-Key topology that can be used to achieve an exact 3^{rd}-order capped reciprocal-Butterworth baseband NGD transfer function translated to a higher center frequency ω_0 (BSF).

Expression (14), associated with translating a 3^{rd}-order reciprocal-Butterworth baseband function with out-of-band gain $A = 100$ (40 dB) and 3 dB cut-off frequency ω_c to a higher center frequency $\omega_0 = 10\omega_c$, is used as an implementation example for the topology in Fig. 5. Parameters of transfer function (14) are summarized as:

$$\omega_{01p} = 10.9046\omega_c, \quad \Delta\omega_{1p} = 1.0864\omega_c,$$
$$\omega_{03p} = 9.1704\omega_c, \quad \Delta\omega_{3p} = 0.9136\omega_c, \quad (17a)$$
$$\omega_{02p} = 14.9294\omega_c, \quad \Delta\omega_{2p} = 6.4081\omega_c,$$
$$\omega_{04p} = 6.6982\omega_c, \quad \Delta\omega_{4p} = 2.875\omega_c, \quad (17b)$$
$$\omega_0 = 10\omega_c, \ \Delta\omega_{5p} = 2\omega_c, \ \Delta\omega_{6p} = 2A^{1/3}\omega_c = 9.2832\omega_c. \quad (17c)$$

The component values of the design in Fig. 5 are obtained by equating the Sallen-Key transfer function (15), with the BSF transfer function (14) and its parameters given by (17a)–(17c). The design component values calculation is demonstrated for a chosen center frequency design at $f_0 = 10f_c = 500$ MHz, thus yielding a bandwidth of $\Delta f = 2f_c = 100$ MHz (20%) in this example. First, a desired input impedance at center frequency is chosen, in this example $Z_{in} \approx 10Z_0 = 500\,\Omega$, such that loading effects are relatively small when a non-buffered source is used (or, if a shunt resistor R_m from Fig. 5 is used to match the design closer to a non-buffered source impedance Z_0 within the bandwidth). Having $Z_{in} \gg Z_0$ ensures that the desired transfer function will not be affected considerably. Circuit component values are then calculated as:

$$R_1 \approx Z_{in} = 500\,\Omega, \quad C_1 = \frac{1}{\Delta\omega_{1p}R_1} = 5.86\,\text{pF},$$
$$L_1 = \frac{1}{\omega_{01p}^2 C_1} = 14.541\,\text{nH}, \quad (18a)$$
$$R_2 = R_1 = 500\,\Omega, \quad C_2 = \frac{1}{\Delta\omega_{3p}R_2} = 6.968\,\text{pF},$$
$$L_2 = \frac{1}{\omega_{03p}^2 C_2} = 17.29\,\text{nH}, \quad (18b)$$
$$R_G = \frac{1/C_1 + 1/C_2}{\Delta\omega_{2p} + \Delta\omega_{4p} - \Delta\omega_{1p} - \Delta\omega_{3p}} = 137.3\,\Omega, \quad (18c)$$
$$R_F = \frac{1}{\left(\omega_{02p}^2 + \omega_{04p}^2 + \Delta\omega_{2p}\Delta\omega_{4p} - \omega_{01p}^2 - \omega_{03p}^2 - \Delta\omega_{1p}\Delta\omega_{3p}\right)R_G C_1 C_2 - \frac{2}{R_1^2}}$$
$$= 24.11\,\Omega, \quad (18d)$$
$$R_3 = Z_0\left(A^{\frac{1}{3}} - 1\right) = 182.08\,\Omega,$$
$$C_3 = \frac{1}{\Delta\omega_{5p}R_3} = 8.741\,\text{pF},$$
$$L_3 = \frac{1}{\omega_0^2 C_3} = 11.592\,\text{nH}. \quad (18e)$$

Sallen-Key topology component value calculations given by expressions (18a)–(18d) are associated with the 2^{nd}-order term of the overall 3^{rd}-order baseband function given by (13), as it translates to the corresponding two terms in the design around center frequency $f_0 = 500$ MHz, as given by (14). Expressions (18a)–(18d) are discussed in more detail in [10]. Tuned frequencies of the two resonators at the op-amp input of the topology in Fig. 5, in this case, are $f_{01p} = 10.9046f_c = 545.23$ MHz, and $f_{03p} = 9.1704f_c = 458.52$ MHz, as given by (17a). The remaining 1^{st}-order term in (13), and its corresponding term in the design around the higher center frequency given by (14), is implemented with a resonator at the op-amp output in Fig. 5. This resonator is tuned at the overall design

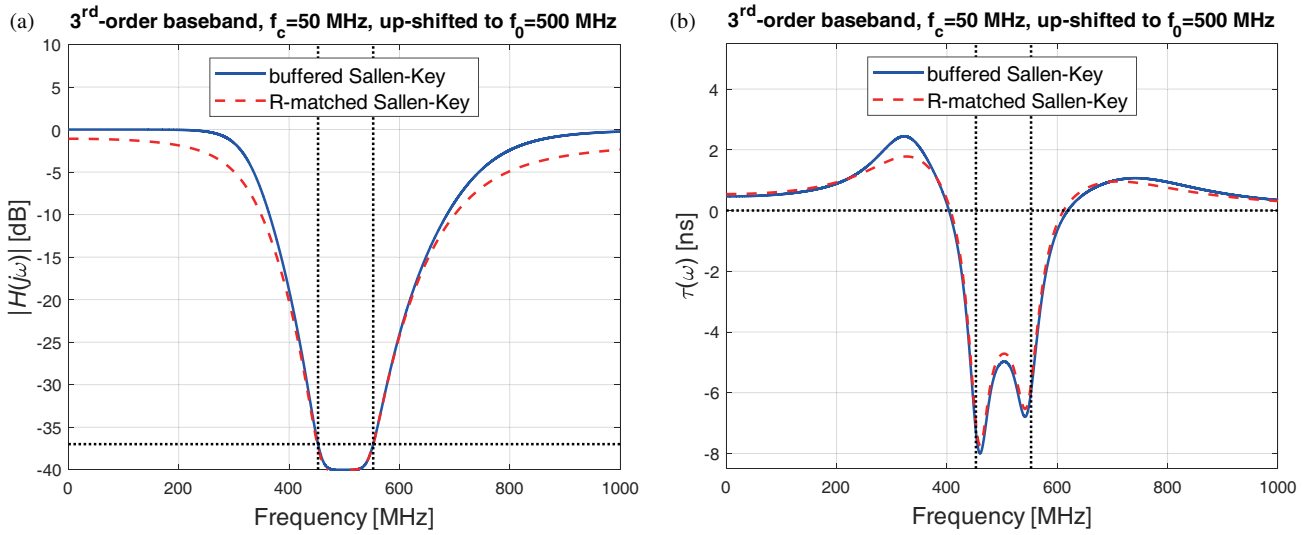

FIGURE 6. Transmission coefficient (a) and group delay (b) of the ideal source (buffered) driven Sallen-Key design, and of the shunt resistor matched design driven by a 50 Ω source.

center frequency $f_0 = 500$ MHz, and the component values are calculated by (18e).

Transfer function magnitude and group delay responses of the topology depicted in Fig. 5 are shown in Fig. 6, for a design driven by an ideal/buffered source, as well as the 50 Ω-source driven design with a shunt matching resistor R_m. Due to the relatively high values of the Z_1 and Z_2 resonator's resistors chosen ($10Z_0 = 500\,\Omega$), resistive match via a shunt resistor ($R_m = 55.56\,\Omega$ used in this example matches R_1 to Z_0, where R_1 approximates the input impedance at ω_{01p}, where it is purely real) yields an in-band match close to the ideal source circuit, as expected and shown in Fig. 6. For the buffered and resistor-matched designs, the 3 dB bandwidths are $552.5 - 452.5 = 100$ MHz and $552.4 - 451.2 = 101.2$ MHz, and the center frequency NGD values are 4.99 ns and 4.73 ns. The resulting NGD-bandwidth products are 0.4995 (the same as in Fig. 4(b)) and 0.4787, respectively. This 5% drop in NGD (or a smaller, 4% drop in NGD-bandwidth product due to increased bandwidth) is attributed to a smaller out-of-band gain of the resistor-matched design due to its transfer function magnitude of roughly -1 dB at the out-of-band extremes as compared with 0 dB of the buffered design. Further, maximum group delay variations over the 3 dB bandwidth relative to center frequency NGD are 60.44% and 63.65%, for the buffered and resistor-matched designs, respectively. As a comparison, a 1^{st}-order low pass Butterworth filter has a 50% group delay variation within 3 dB bandwidth, relative to its center frequency positive group delay. A combined in-band amplitude/phase distortion metric is discussed in more detail in Section 9 and applied to selected time-domain waveforms propagation through the proposed design.

Sensitivity analysis for a 1% change in the component values of the circuit in Fig. 5 was conducted, yielding the worst-case deviation of 2.6% in the center frequency, 4.5% in the maximum attenuation, and 14% in the center frequency NGD. Additionally, it should be noted that as design frequency is decreased, both the inductor and capacitor values increase inversely proportional with frequency and may become challenging for implementation below a certain design frequency. A design at the same 500 MHz center frequency and 100 MHz bandwidth, involving an op-amp and a single resonator (compared to 3 resonators in Fig. 5) was fabricated [8]. The design presented here is mostly intended as a proof-of-concept implementation of the proposed transfer function.

4.1. Sallen-Key Implementation of the 5th-Order Baseband Design Translated to Higher Center Frequency

A 5^{th}-order reciprocal-Butterworth baseband design given by expression (3e) and scaled by $1/A$, after it is translated to a higher center frequency design by applying (8) can be implemented by a cascaded Sallen-Key topology shown in Fig. 7. Similar transfer function factorization as the one given by (14) for the 3^{rd}-order baseband design upshifted to a higher center frequency can be conducted for the upshifted 5^{th}-order baseband design analyzed here, resulting in two additional 2^{nd}-order rational factors. The numerators of the two additional factors are tuned at frequencies ω_{05p} and ω_{07p} around the center frequency ω_0 and need an additional Sallen-Key stage compared to the upshifted 3^{rd}-order design, as labeled in Fig. 7.

Applying expressions (18a)–(18d) yields the following component values for the first Sallen-Key circuit in Fig. 7: $R_1 = 500\,\Omega$, $C_1 = 9.409$ pF, $L_1 = 8.905$ nH, $R_2 = 500\,\Omega$, $C_2 = 11.379$ pF, $L_2 = 10.767$ nH, $R_{G1} = 330.7\,\Omega$, $R_{F1} = 14.24\,\Omega$. Similarly, applying expressions equivalent to (18a)–(18d), where ω_{01p} and ω_{03p} are replaced by ω_{05p} and ω_{07p}, respectively, and so on, yields the following component values for the second Sallen-Key circuit in Fig. 7: $R_3 = 500\,\Omega$, $C_3 = 3.716$ pF, $L_3 = 24.236$ nH, $R_4 = 500\,\Omega$, $C_4 = 4.181$ pF, $L_4 = 27.264$ nH, $R_{G2} = 330.7\,\Omega$, $R_{F2} = 147.7\,\Omega$. Finally, applying expressions equivalent to (18e) yields the following component values for the output resonator in Fig. 7: $R_5 = 75.59\,\Omega$, $C_5 = 21.054$ pF, $L_5 = 4.813$ nH.

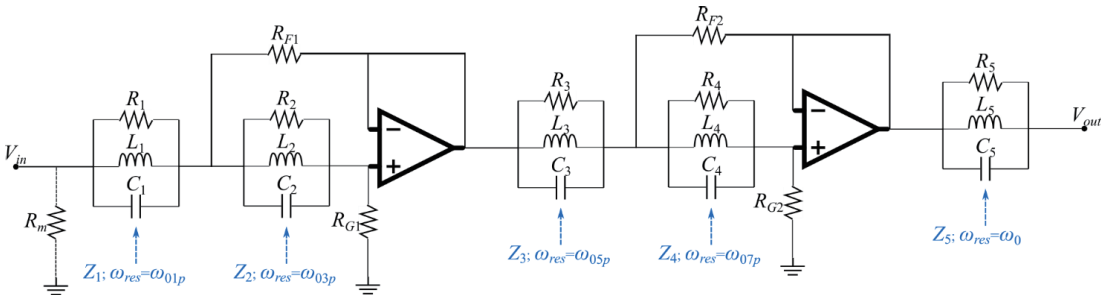

FIGURE 7. Sallen-Key cascaded topology that can be used to achieve an exact 5^{th}-order capped reciprocal-Butterworth baseband NGD transfer function translated to a higher center frequency ω_0 (BSF).

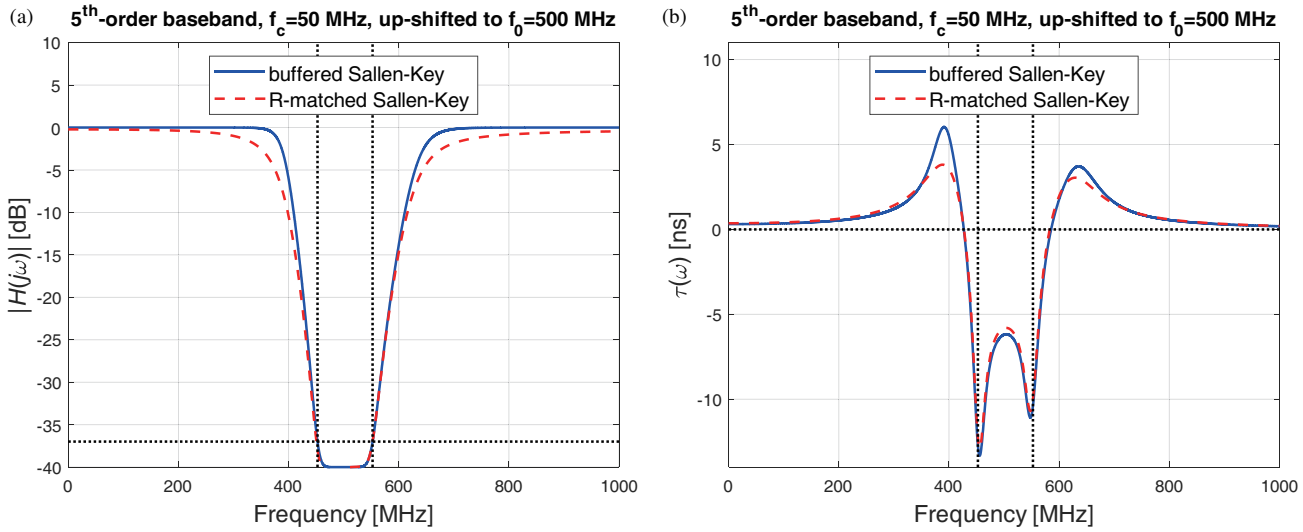

FIGURE 8. Transmission coefficient (a) and group delay (b) of the ideal source (buffered) driven Sallen-Key design, and of the shunt resistor matched design driven by a 50 Ω source.

Transfer function magnitude and group delay responses of the topology depicted in Fig. 7 are shown in Fig. 8, for a design driven by an ideal/buffered source as well as the 50 Ω-source driven design with a shunt matching resistor R_m. The center frequency NGD values shown in Fig. 8(b) for the 5^{th}-order buffered and 50 Ω-source driven design are 6.2 ns and 5.82 ns, respectively (an improvement from the 3^{rd}-order design values of 4.99 ns and 4.73 ns, respectively, shown in Fig. 6(b) for the same out-of-band gain and bandwidth).

5. APPROXIMATE IMPLEMENTATION WITH PASSIVE LADDER CIRCUIT TOPOLOGY

As discussed in the previous section, a Sallen-Key topology can achieve the exact upshifted frequency design transfer function, such as the one given by expression (14). An attempt to provide gain-compensation via the same op-amps in Figs. 5 and 7 (by adding two resistors of a certain ratio at the negative input terminal, one to the ground and one to the output terminal replacing the shorted connection) would result in a considerable distortion of the original transfer function. Therefore, the presented Sallen-Key designs have an attenuation at the center frequency just like a purely passive network would have.

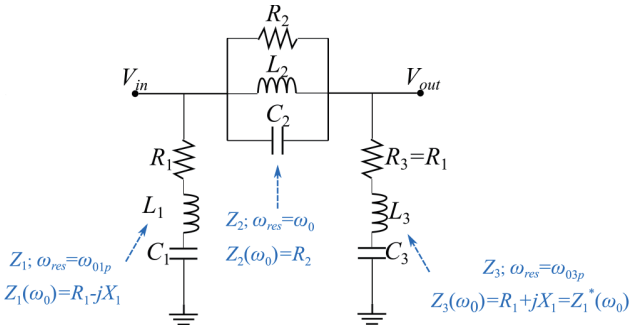

FIGURE 9. Three-resonator π-circuit ladder topology that can achieve an approximate 3^{rd}-order baseband capped reciprocal-Butterworth NGD transfer function translated to a higher center frequency ω_0 (BSF).

Alternatively, all-passive topologies involving resonators (parallel resonators connected in series, and/or series resonators connected in shunt) can potentially achieve relatively good match to the exact transfer function, such as the one given by (14). Fig. 9 illustrates a three-resonator π-circuit, which can achieve an approximate implementation of the transfer function given by (14). This circuit can also be transformed into its T-circuit equivalent, such that series resonators connected

in shunt would be replaced by parallel resonators connected in series, and vice versa. The relationship between equivalent series and parallel resonators components can be derived as: $R_p = Z_0^2/R_s$, $L_p = Z_0^2 \cdot C_s$, and $C_p = L_s/Z_0^2$, which also yields $Z_p(\omega) = Z_0^2/Z_s(\omega)$.

The transfer function of the design shown in Fig. 9, assuming that it is driven by a Z_0-impedance source and terminated in a Z_0-impedance load, is given by:

$$H(j\omega) = \frac{V_{out}}{V_{in}} = \frac{2}{(1+Z_2/Z_0+Z_2/Z_3)\cdot(1+Z_0/Z_1)+(1+Z_0/Z_3)}. \quad (19)$$

After expanding transfer function (19) impedances into their frequency dependent components, it can be shown that it becomes a 6^{th}-order rational transfer function of frequency. When (19) is factorized into three 2^{nd}-order product terms, it becomes clear that the numerator can be matched exactly to the transfer function (14), by selecting the three resonators' center frequencies to match the corresponding ones in (14), as labeled in Fig. 9. Further, for the numerators of expressions (14) and (19) to match, the three resonators' bandwidths also need to be matched to the corresponding ones in (14), as: $\Delta\omega_{1p} = R_1/L_1$, $\Delta\omega_{5p} = 1/(R_2C_2)$, and $\Delta\omega_{3p} = R_3/L_3$. The matched numerator parameter values between (14) and (19) are:

$$\begin{aligned}
&\omega_{01p} = \omega_{01\pi} = 10.9046\omega_c,\\
&\Delta\omega_{1p} = \Delta\omega_{1\pi} = 1.0864\omega_c,\\
&\omega_{03p} = \omega_{03\pi} = 9.1704\omega_c,\\
&\Delta\omega_{3p} = \Delta\omega_{3\pi} = 0.9136\omega_c,\\
&\omega_{05p} = \omega_{05\pi} = \omega_0 = 10\omega_c,\\
&\omega_{5p} = \Delta\omega_{5\pi} = 2\omega_c.
\end{aligned} \quad (20)$$

With the transfer function numerator matching of (14) and (19) in mind, the remaining degrees of freedom in Fig. 9 topology are the three resonators resistor values. Further, it can be shown that to satisfy the transfer function value requirement at the center frequency $H(j\omega_0) = 1/A$, a purely real number, shunt impedances Z_1 and Z_3 need to have their imaginary parts equal in magnitude and opposite in sign, at ω_0. This is only possible if $R_3 = R_1$, as shown below by employing expressions (10), and as labeled accordingly in Fig. 9:

$$X_1 = -\mathrm{Im}\{Z_1(\omega_0)\} = \frac{1}{\omega_0 C_1} - \omega_0 L_1 = \left(\frac{\omega_{01p}^2}{\omega_0} - \omega_0\right)\frac{R_1}{\Delta\omega_{1p}}, \quad (21a)$$

$$X_3 = \mathrm{Im}\{Z_3(\omega_0)\} = \left(\omega_0 - \frac{\omega_{03p}^2}{\omega_0}\right)\frac{R_3}{\Delta\omega_{3p}} = = \left(\omega_0 - \frac{\omega_0^3}{\omega_{01p}^2}\right)\frac{\omega_{01p}^2}{\omega_0^2}\frac{R_1}{\Delta\omega_{1p}} = X_1. \quad (21b)$$

Further, for the transfer function attenuation at the center frequency to be exactly $H(j\omega_0) = 1/A$, it can be derived that the middle resonator resistance is not independent, and instead given by:

$$R_2 = 2\frac{(A-1)\left(R_1^2+X_1^2\right) - Z_0R_1}{\left(R_1^2+X_1^2\right)/Z_0 - 2R_1 + Z_0} \quad (22)$$

From (22), the only degree of freedom is the shunt resonators' resistance value R_1, given the match of the numerator of (19) to the numerator of the capped reciprocal-Butterworth NGD transfer function (14), and given required center frequency attenuation of $1/A$.

As depicted in Fig. 10, varying the only degree of freedom value, R_1, does not result in a single value that yields an exact simultaneous match of all denominator parameters of the π-circuit transfer function (19) to those of the exact transfer function (14).

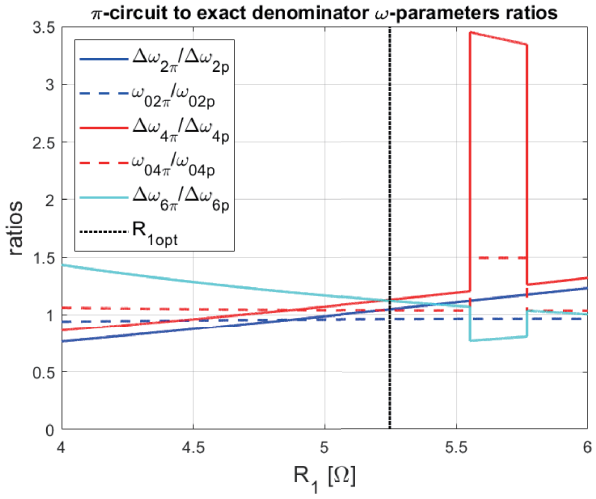

FIGURE 10. Ratios of π-circuit transfer function denominator parameters to the ratios to corresponding parameters of an exact capped reciprocal-Butterworth transfer function, as a function of resistor value R_1.

Since the exact transfer function match is not possible with this topology, an additional optimization criterion is needed to ensure a good in-band transfer function match. Since a characteristic of Butterworth filters has magnitude response flatness within a frequency band of interest, that feature is selected here to determine the optimal value R_1. Thus, by selecting the magnitude response curvature, or 2^{nd} derivative, closest to zero at the center frequency, an optimal value $R_1 = 5.2468\,\Omega$ is obtained in this example, as also labeled by a vertical line in Fig. 10 (a reasonable initial guess value for R_1 corresponds to a single shunt resonator design which would have a center frequency attenuation of $1/A^{1/3}$, i.e., $R_{1-initial} = Z_0/(2(A^{1/3}-1)) = 6.865\,\Omega$). The center-frequency-flatness optimized π-circuit transfer function yields the following denominator parameters of transfer function (19), as compared to the exact ones in (14):

$$\begin{aligned}
&\omega_{02\pi} = 14.3763\omega_c, \quad \Delta\omega_{2\pi} = 6.7119\omega_c,\\
&\omega_{04\pi} = 6.9559\omega_c, \quad \Delta\omega_{4\pi} = 3.2475\omega_c,
\end{aligned} \quad (23a)$$

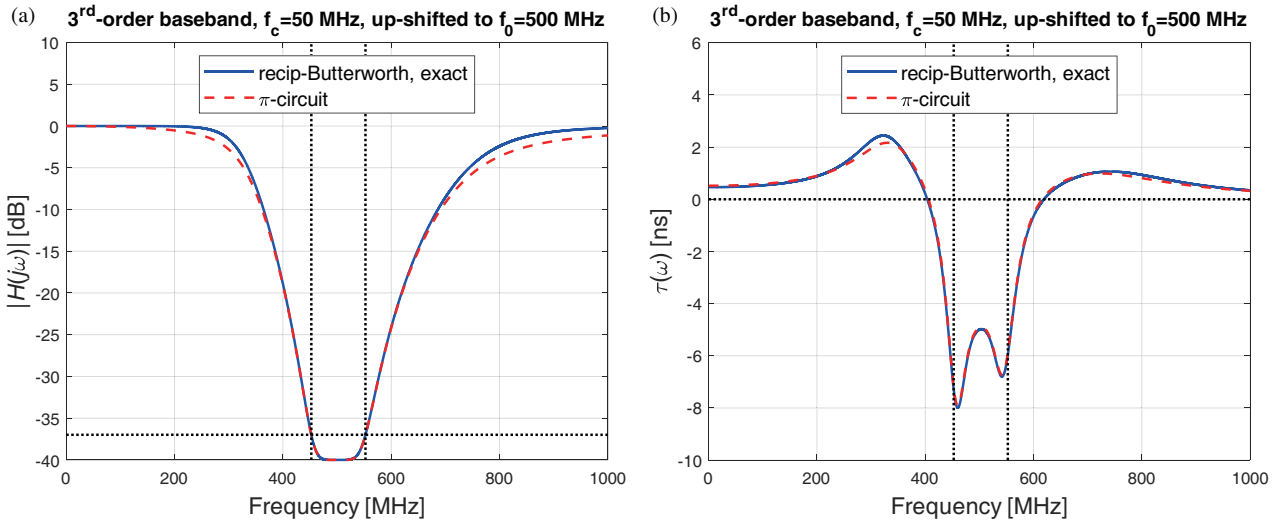

FIGURE 11. Transmission coefficient (a) and group delay (b) of the exact capped reciprocal-Butterworth 3^{rd}-order design upshifted to a higher center frequency, and of the π-circuit all-passive design.

$$\omega_{02p} = 14.9294\omega_c, \quad \Delta\omega_{2p} = 6.4081\omega_c,$$
$$\omega_{04p} = 6.6982\omega_c, \quad \Delta\omega_{4p} = 2.875\omega_c, \tag{23b}$$
$$\Delta\omega_{6\pi} = 10.408\omega_c, \quad \Delta\omega_{6p} = 9.2832\omega_c,$$
$$\omega_{06\pi} = \omega_{06p} = \omega_0 = 10\omega_c. \tag{23c}$$

Substituting the optimized $R_1 = 5.2468\,\Omega$ value into expressions (21a) and (22) yields $X_1 = 9.133\,\Omega$ and $R_2 = 341.8909\,\Omega$, respectively. All component values, corresponding to the design in Fig. 9 in this example with $A = 100$, $f_0 = 500$ MHz, $f_c = 50$ MHz, are:

$$R_1 = 5.2468\,\Omega, \quad L_1 = \frac{1}{\Delta\omega_{1p}R_1} = 15.373\,\text{nH},$$
$$C_1 = \frac{1}{\omega_{01p}^2 L_1} = 5.5428\,\text{pF}, \tag{24a}$$
$$R_3 = 5.2468\,\Omega, \quad L_3 = \frac{1}{\Delta\omega_{3p}R_3} = 18.281\,\text{nH},$$
$$C_3 = \frac{1}{\omega_{03p}^2 L_3} = 6.5908\,\text{pF}, \tag{24b}$$
$$R_2 = 341.8909\,\Omega, \quad C_2 = \frac{1}{2\omega_c R_2} = 4.6551\,\text{pF},$$
$$L_2 = \frac{1}{\omega_0^2 C_2} = 21.765\,\text{nH}. \tag{24c}$$

Transfer function magnitude and group delay responses of the topology depicted in Fig. 9 are shown in Fig. 11. The center frequency NGD values shown in Fig. 11(b) for the 3^{rd}-order exact and π-circuit designs are 4.99 ns and 4.93 ns, respectively. Therefore, the three-resonator π-circuit shows an even better match to the exact transfer function, compared to a non-ideal source driven Sallen-Key topology (which has center frequency NGD of 4.73 ns, as per Fig. 6(b)). Sensitivity for a 1% change in the component values of the all-passive circuit in Fig. 9 is very similar to that of the Sallen-Key design in Fig. 5 (worst-case deviation of 14.4% in the center frequency NGD). As a comparison, a classical Butterworth bandpass ladder design of the same order, center frequency, and bandwidth would have a worst-case 2.4% deviation of the center frequency (positive) group delay.

5.1. Ladder Implementation of the 5th-Order Baseband Design Translated to a Higher Center Frequency

A 5^{th}-order capped reciprocal-Butterworth baseband design translated to a higher center frequency can be approximately implemented by an all-passive five-resonator ladder topology shown in Fig. 12. Following similar derivations to those associated with the three-resonator π-circuit design, it can be shown that to match the numerator of the exact 5^{th}-order transfer function upshifted to higher center frequency, the resonators in Fig. 12 need to have their center frequencies and bandwidths matched to those detailed in Subsection 4.1 for the Sallen-Key design. Further, for the center frequency attenuation to be exactly $1/A$, it can be shown via derivations similar to (21a)–(21b) that $R_5 = R_1$ and $R_4 = R_2$ conditions need to be met, which in turn yield center frequency complex conjugate impedance values of corresponding resonators, as labeled in Fig. 12. Therefore, the two degrees of freedom are resistors R_1 and R_2, which after applying the optimization for the maximum magnitude response flatness at the center frequency, yield optimized values $R_1 = R_5 = 6.69\,\Omega$ and $R_2 = R_4 = 162.92\,\Omega$ (reasonable initial guess values for R_1 and R_2 correspond to a single resonator shunt and series design, respectively, each having a center frequency attenuation of $1/A^{1/5}$, i.e., $R_{1-initial} = Z_0/(2(A^{1/5} - 1)) = 16.54\,\Omega$ and $R_{2-initial} = Z_0 \cdot 2(A^{1/5} - 1) = 151.19\,\Omega$).

Further, for the transfer function attenuation at the center frequency to be exactly $H(j\omega_0) = 1/A$, it can be shown that the middle resonator resistance can be calculated from the other resonators' parameters, yielding $R_3 = 16.72\,\Omega$. With

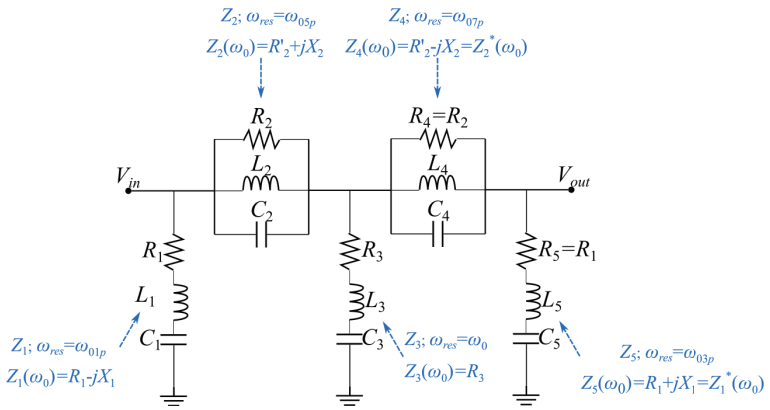

FIGURE 12. Five-resonator ladder topology that can be used to achieve an approximate 5^{th}-order baseband capped reciprocal-Butterworth NGD transfer function translated to a higher center frequency ω_0 (BSF).

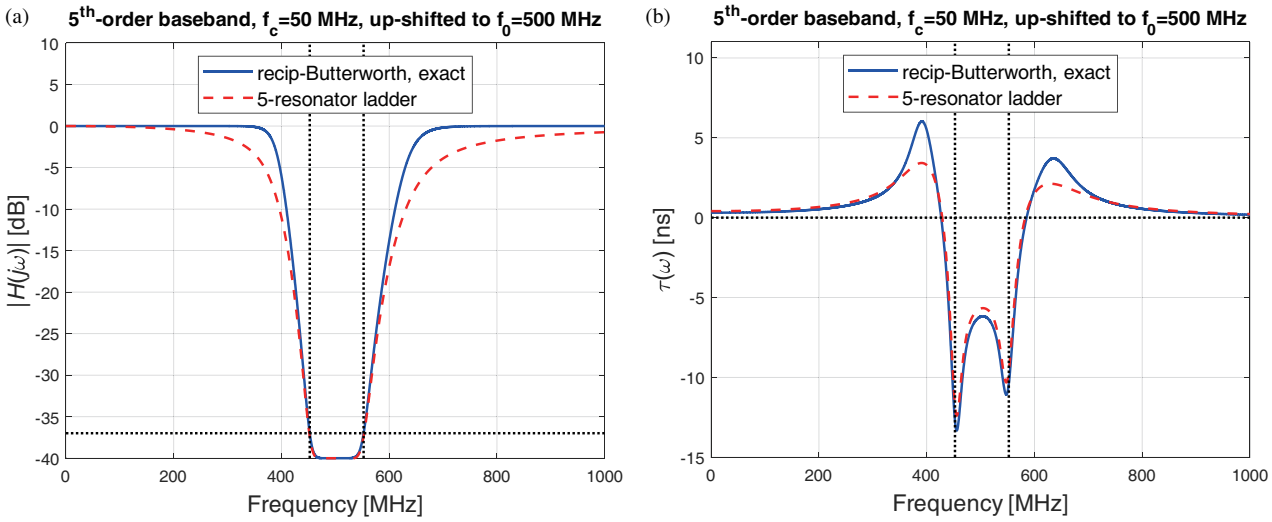

FIGURE 13. Transmission coefficient (a) and group delay (b) of the exact capped reciprocal-Butterworth 5^{th}-order design upshifted to a higher center frequency, and of the all-passive five-resonator ladder design.

all five resonators' resistances determined, expressions similar to (24a)–(24c) can be used to calculate the remaining components values from Fig. 12: $C_1 = 2.662\,\text{pF}$, $L_1 = 31.473\,\text{nH}$, $C_2 = 11.404\,\text{pF}$, $L_2 = 7.897\,\text{nH}$, $C_3 = 3.808\,\text{pF}$, $L_3 = 26.611\,\text{nH}$, $C_4 = 12.83\,\text{pF}$, $L_4 = 8.885\,\text{nH}$, $C_5 = 3.219\,\text{pF}$, $L_5 = 38.061\,\text{nH}$.

Transfer function magnitude and group delay responses of the topology depicted in Fig. 12 and those of the exact capped reciprocal-Butterworth 5^{th}-order design upshifted to a higher center frequency are shown in Fig. 13. The center frequency NGD values shown in Fig. 13(b) for the 5^{th}-order exact reciprocal-Butterworth transfer function and the five-resonator design from Fig. 12 are 6.2 ns and 5.69 ns, respectively.

6. NGD-BANDWIDTH PRODUCT ASYMPTOTIC LIMIT OF AN Nth-ORDER RECIPROCAL-BUTTERWORTH DESIGN

Similar to the design with cascaded 1^{st}-order stages [8, 9], or 2^{nd}-order stages [10], it is useful to express the NGD-bandwidth product of the N^{th}-order capped reciprocal-Butterworth design presented here as a function of the out-of-band gain trade-off quantity. As discussed in [8–10], in addition to causing a center frequency attenuation for a passive design, the out-of-band gain in the frequency domain is directly proportional to the magnitude of undesired transients in the time domain, when waveforms/pulses with defined turn-on/off instances (associated with signal modulation during information transmission) are propagated.

Due to symmetry in the sine function around $\pi/2$, center frequency NGD expressions (7a) and (7b) for even or odd orders of the baseband capped reciprocal-Butterworth design, respectively, can be expressed via a single expression for any order N, as:

$$\text{NGD} \cdot \Delta f = -\tau\,(0) \cdot \frac{2\omega_c}{2\pi} =$$

$$\frac{1}{\pi}\frac{1}{C_{\omega-3\,\text{dB}}}\left(1-\frac{1}{A^{1/N}}\right)\sum_{k=1}^{N}\sin\left(\frac{2k-1}{2N}\pi\right), \quad (25)$$

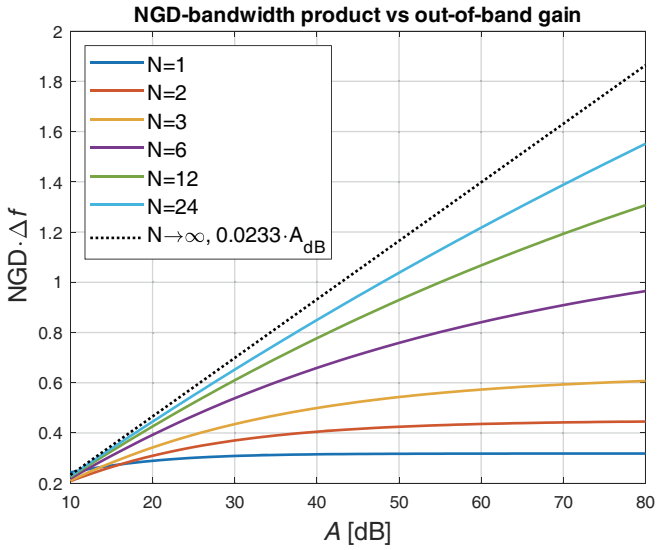

FIGURE 14. NGD-bandwidth product for N^{th}-order baseband capped reciprocal-Butterworth designs, as a function of overall out-of-band gain.

where the 3 dB bandwidth correction factor $C_{\omega-3\,\mathrm{dB}}$ is given by (6). The NGD-bandwidth product for several N^{th}-order baseband capped reciprocal-Butterworth designs, as a function of out-of-band gain, is plotted in Fig. 14 based on expression (25). For each finite order N, NGD-bandwidth product has an upper limit as out-of-band gain approaches infinity (as $A \to \infty$, $C_{\omega-3\,\mathrm{dB}}$ and $1 - 1/A^{1/N}$ both approach 1.0, and (25) yields upper limits of $1/\pi \approx 0.3183$, $\sqrt{2}/\pi \approx 0.4502$, $2/\pi \approx 0.6366$, for $N = 1$, 2, 3, respectively, and so on).

Alternatively, for high values of order N, it is beneficial to rewrite the sum in expression (25) in this form:

$$\begin{aligned} S(N) &= \sum_{k=1}^{N} \sin\left(\frac{2k-1}{2N}\pi\right) \\ &= \frac{N}{\pi}\sum_{k=1}^{N} \sin\left(\frac{2k-1}{2N}\pi\right)\frac{\pi}{N} \\ &= \frac{N}{\pi}\sum_{k=1}^{N} \sin(x_k)\,\Delta x, \end{aligned} \tag{26a}$$

where $x_k = (2k-1)\pi/(2N)$, and $\Delta x = x_{k+1} - x_k = \pi/N$. As order N increases, discrete variable x_k in (26a) tends to a continuous variable x with lower/upper bounds (0, π); the difference between consecutive x_k values tends to become infinitesimal $\Delta x \to dx$; therefore, the discrete sum in (26a) becomes an integral, evaluated as:

$$\lim_{N\to\infty} S(N) = \frac{N}{\pi}\int_0^{\pi} \sin(x)\,dx = \frac{2N}{\pi}. \tag{26b}$$

By substituting (26b) into (25), the NGD-bandwidth product as the order N approaches infinity, as a function of finite out-of-band gain, becomes (as $N \to \infty$, $C_{\omega-3\,\mathrm{dB}}$ approaches 1.0):

$$\begin{aligned} \lim_{N\to\infty}(\mathrm{NGD}\cdot\Delta f) &= \lim_{N\to\infty}\left(\left(1-\frac{1}{A^{1/N}}\right)\cdot\frac{2N}{\pi^2}\right) \\ &= \frac{2}{\pi^2}\lim_{N\to\infty}\left(\left(e^{\ln(A)/N}-1\right)\cdot N\right) \\ &= \frac{2\ln(A)}{\pi^2}, \end{aligned} \tag{27}$$

or, as a function of the out-of-band gain given in decibels, $A_{\mathrm{dB}} = 20\cdot\log(A)$, NGD-bandwidth becomes a linear asymptotic function, as also depicted in Fig. 14:

$$\begin{aligned} \lim_{N\to\infty}(\mathrm{NGD}\cdot\Delta f) &= \frac{2}{\pi^2}\frac{10\log(A)}{10\log(e)} = \frac{\ln(10)}{10\pi^2}A_{\mathrm{dB}} \\ &\approx 0.0233\cdot A_{\mathrm{dB}}. \end{aligned} \tag{28}$$

7. NGD-BANDWIDTH PRODUCT ASYMPTOTIC LIMIT OF CASCADED LOWER-ORDER RECIPROCAL-BUTTERWORTH STAGES

For a given overall order of a rational transfer function based on the proposed capped reciprocal-Butterworth design, it is worthwhile comparing a single transfer function design of that same order, against a cascaded lower order transfer function design (for example, two cascaded transfer functions each with a half of the overall order, given that the overall order is an even number). In general, for n cascaded capped reciprocal-Butterworth transfer functions of N^{th}-order, with the overall out-of-band gain A (each of the n stages has an individual out-of-band gain of $A^{1/n}$), the 3 dB bandwidth correction factor from expression (6) can be augmented to be (substituting $n = 1$ yields the original expression for a single N^{th}-order transfer function):

$$C_{\omega-3\,\mathrm{dB}} = \left(\frac{1-\left(\frac{2}{A^2}\right)^{1/n}}{2^{1/n}-1}\right)^{\frac{1}{2N}}. \tag{29}$$

The NGD-bandwidth product for this cascaded design becomes a modified version of (25), with each of the n stages having an individual out-of-band gain of $A^{1/n}$, and the observed center frequency NGD becomes a multiple of n individual stage NGD values:

$$\mathrm{NGD}\cdot\Delta f = \frac{n}{\pi}\frac{1}{C_{\omega-3\,\mathrm{dB}}}\left(-\frac{1}{A^{1/(n\cdot N)}}\right)\sum_{k=1}^{N}\sin\left(\frac{2k-1}{2N}\pi\right). \tag{30}$$

NGD-bandwidth product for variations of a 6^{th}-order baseband reciprocal-Butterworth design ($n \times N^{th} = 1\times 6^{th}$, 2×3^{rd}, 3×2^{nd}, 6×1^{st}), as a function of out-of-band gain is plotted in Fig. 15 based on expression (30), with the 3 dB correction factor given by (29). It is clear from Fig. 15 that a single stage of higher order capped reciprocal-Butterworth design exhibits a higher NGD-bandwidth product than any cascaded version with lower order designs that yield the same overall order. However,

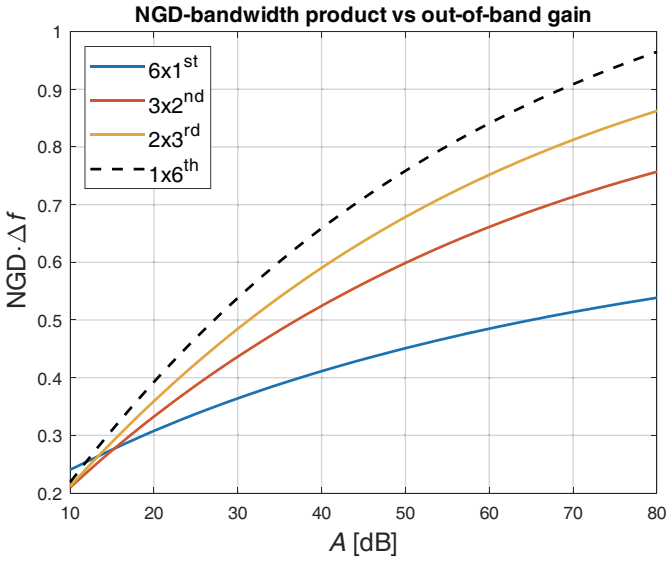

FIGURE 15. NGD-bandwidth product for variations of a 6^{th}-order baseband capped reciprocal-Butterworth design (1×6^{th}, 2×3^{rd}, 3×2^{nd}, and 6×1^{st}), as a function of overall out-of-band gain.

cascaded designs can have a smaller phase and group delay distortion associated with them, as evident from Fig. 2(b). Further, the periodic nature of cascaded identical stages enables a characteristic impedance of the design to be defined, which makes it suitable for studies involving distributed medium analysis. When the number of stages becomes large, the transfer function becomes an exponential function which is a characteristic of physical media, as analyzed in [8, 9] for 1^{st}-order, and in [10] for 2^{nd}-order cascaded designs.

For distributed ($n \to \infty$) cascaded N^{th}-order reciprocal-Butterworth transfer functions, the limit of the 3 dB bandwidth correction factor (29) becomes:

$$C_{\omega-3\,\mathrm{dB}-inf} = \lim_{n\to\infty}\left(C_{\omega-3\,\mathrm{dB}}\right) = \left(\frac{2\ln(A)}{\ln 2} - 1\right)^{\frac{1}{2N}}, \quad (31)$$

and the NGD-bandwidth product from expression (30) becomes (the final approximated result assumes that the overall out-of-band gain is much larger than the 3 dB gain at bandwidth edges, i.e., $A \gg 2^{1/2}$, or $2\ln(A) \gg \ln 2$):

$$\lim_{n\to\infty}(\mathrm{NGD}\cdot\Delta f) = \frac{1}{\pi}\left(\frac{\ln 2}{2\ln(A) - \ln 2}\right)^{\frac{1}{2N}}$$
$$\cdot \sum_{k=1}^{N}\sin\left(\frac{2k-1}{2N}\pi\right)\cdot\lim_{n\to\infty}\left(n\frac{A^{1/(n\cdot N)}-1}{A^{1/(n\cdot N)}}\right)$$
$$\approx \frac{1}{\pi N}\left(\frac{\ln 2}{2}\right)^{\frac{1}{2N}}\left(\frac{\ln 10}{20}\right)^{\left(1-\frac{1}{2N}\right)}\sum_{k=1}^{N}\sin\left(\frac{2k-1}{2N}\pi\right)A_{\mathrm{dB}}^{\left(1-\frac{1}{2N}\right)}. \quad (32)$$

The NGD-bandwidth product asymptotic limit for several distributed designs with cascaded stages of certain order can be computed from (32), yielding:

$$(\mathrm{NGD}\cdot\Delta f)_{distr-1^{st}} \approx \frac{1}{\pi}\sqrt{\left(\frac{\ln 2}{2}\right)\left(\frac{\ln 10}{20}\right)}\sqrt{A}_{\mathrm{dB}}$$
$$\approx 0.0636\cdot\sqrt{A}_{\mathrm{dB}}, \quad (33a)$$

$$(\mathrm{NGD}\cdot\Delta f)_{distr-2^{nd}} \approx \frac{1}{\pi}\frac{1}{\sqrt{2}}\left(\frac{\ln 2}{2}\right)^{1/4}\left(\frac{\ln 10}{20}\right)^{3/4}A_{\mathrm{dB}}^{3/4}$$
$$\approx 0.0341\cdot A_{\mathrm{dB}}^{3/4}, \quad (33b)$$

$$(\mathrm{NGD}\cdot\Delta f)_{distr-3^{rd}} \approx \frac{2}{3\pi}\left(\frac{\ln 2}{2}\right)^{1/6}\left(\frac{\ln 10}{20}\right)^{5/6}A_{\mathrm{dB}}^{5/6}$$
$$\approx 0.0294\cdot A_{\mathrm{dB}}^{5/6}, \quad (33c)$$

$$(\mathrm{NGD}\cdot\Delta f)_{distr-4^{th}} \approx 0.0275\cdot A_{\mathrm{dB}}^{7/8}, \quad (33d)$$

$$(\mathrm{NGD}\cdot\Delta f)_{distr-5^{th}} \approx 0.0265\cdot A_{\mathrm{dB}}^{9/10}, \quad (33e)$$

$$\lim_{N\to\infty}\left((\mathrm{NGD}\cdot\Delta f)_{distr-N^{th}}\right)$$
$$\approx \frac{\ln(10)}{10\pi^2}A_{\mathrm{dB}} \approx 0.0233\cdot A_{\mathrm{dB}}. \quad (33f)$$

Derived asymptotic expressions (33a)–(33f) for distributed ($n \to \infty$) designs are plotted in Fig. 16, along with their exact expression (30) counterparts, evaluated for a large number of cascaded stages ($n = 30$ in this example), showing good agreement. Expression (33a) is identical to the one derived in [8, 9], since reciprocal-Butterworth design proposed in this paper, for 1^{st}-order case, is identical to the transfer functions in the previous work. Similarly, expression (33b) is identical to the one in [10] since 2^{nd}-order cascaded functions are identical as well. Third-order expression (33c) and higher order expressions of the distributed designs show the extension of the trend of the previous work, with the overall power of $(1 - 1/(2N))$ relationship between the NGD-bandwidth product and the decibel value of out-of-band gain. Eventually, as the order of distributed cascaded stages approaches infinity, the relationship tends to a linear one given by (33f), which is also identical to

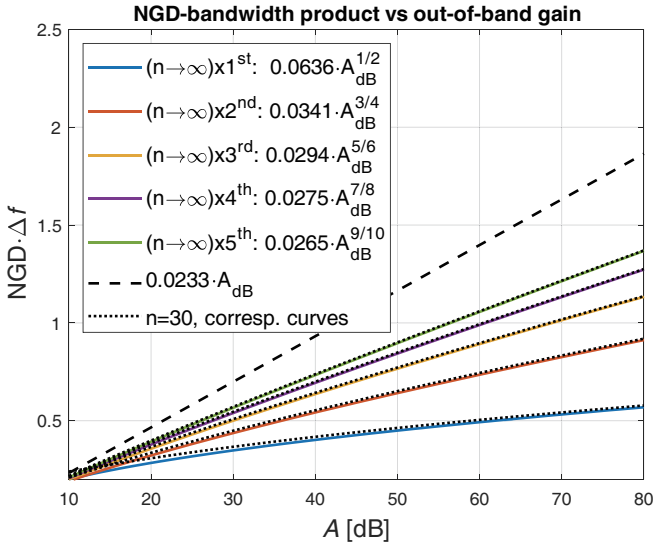

FIGURE 16. NGD-bandwidth product for several distributed ($n \to \infty$) cascaded N^{th}-order stages, as a function of overall out-of-band gain.

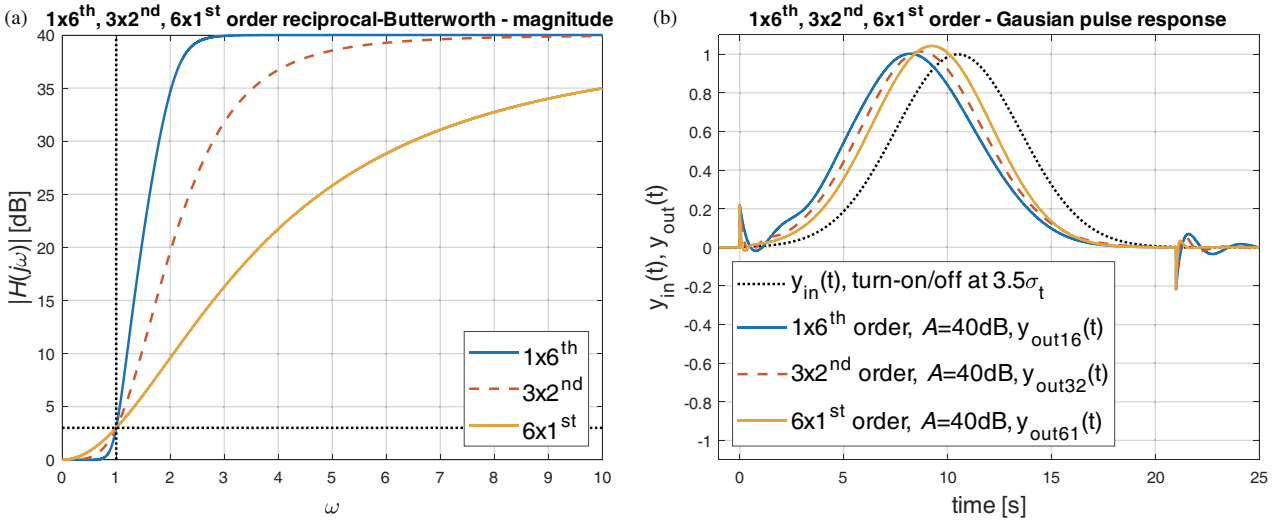

FIGURE 17. Reciprocal-Butterworth 1×6^{th}, 3×2^{nd} and 6×1^{st}-order baseband designs with 40 dB out-of-band gain (a) magnitude responses, and (b) time-domain responses to a Gaussian pulse turned-on/off at $3.5\sigma_t$.

expression (28) of a single stage of reciprocal-Butterworth design of an order approaching infinity (cascading a design of an infinite order is not possible, and it reduces to a single stage of that infinite order).

8. RELATIONSHIP BETWEEN TIME DOMAIN AND FREQUENCY DOMAIN NGD METRICS

A main trade-off quantity associated with NGD designs is the frequency domain out-of-band gain, manifested in the magnitude response outside the NGD bandwidth being higher than that within it. This results in signal attenuation (SA) for gain-uncompensated designs. Further, there is a proportional relationship between the out-of-band gain and the amplitude of transients in the time domain, when information carrying signals such as pulses with finite turn-on/off times propagate in an NGD medium [8, 9]. More generally, any nonanalytic discontinuities in the propagated pulse or its derivatives are essentially information carriers and will generate a transient response by the medium [12]. The transient's magnitude amplification phenomenon is demonstrated for the example of a Gaussian pulse with finite turn-on/off times, which is propagated through selected variations of the capped reciprocal-Butterworth NGD designs. A qualitative explanation of the transient amplification phenomenon first considers that truncating a continuous waveform in time will result in a larger portion of the pulse spectral power being contained outside the NGD bandwidth, as compared to the corresponding continuous waveform alone. The extended power spectrum of the time-truncated waveform will then be amplified by the out-of-band gain of an NGD medium, resulting in increased transient amplitude.

For NGD designs exhibiting the same out-of-band gain, the same amplitude of transients is expected. This is shown in Fig. 17(b) for 1×6^{th}, 3×2^{nd}, and 6×1^{st}-order capped reciprocal-Butterworth baseband designs. All three example designs are chosen to have an out-of-band gain of 40 dB ($A = 100$), with center frequency magnitude response fully gain-compensated (0 dB). The input signal chosen to evaluate the NGD designs shown in Fig. 17 is a Gaussian pulse with its frequency spectrum standard deviation corresponding to 1/3 of the NGD designs' 3 dB bandwidth cut-off frequency ($\sigma_\omega = \omega_c/3 = 1/3$), and the turn-on/off times chosen at $3.5\sigma_t$ ($\sigma_t = 1/\sigma_\omega$). The input pulse value at the selected turn-on/off times is $\exp(-3.5^2/2) \approx 0.0022$ of the peak value. Subsequently, the transient amplitude is expected to be amplified by $A = 100$, which is 0.22 of the peak value, as corroborated in Fig. 17(b). Therefore, referring to Fig. 15 which shows the NGD-bandwidth product for different designs, we can conclude that for the same out-of-band-gain and thus the same transient amplitude, a 1×6^{th}-order design can achieve a larger pulse peak advancement than a 3×2^{nd}-order design and an even larger advancement than a 6×1^{st}-order design. The transient settling time, however, is the longest for the 1×6^{th}-order design and progressively decreases for the 3×2^{nd}-order and 6×1^{st}-order designs, as observed after the turn-off time in Fig. 17(b). The longer transient settling time and higher successive amplitudes of the decaying oscillation are a result of the steeper magnitude characteristic transition from in-band to out-of-band.

The center frequency NGD value in the frequency domain is expected to be relatively close to the pulse-peak time advancement in the time domain, with the difference proportional to transfer function magnitude and group delay variations within the bandwidth where most of the applied pulse frequency spectrum power is contained. For example, from Fig. 15, at 40 dB out-of-band gain, 1×6^{th}, 3×2^{nd}, and 6×1^{st}-order designs have NGD-bandwidth product values of NGD$\cdot\Delta f = 0.659$, 0.5245, and 0.4113, respectively, which for a bandwidth of $\Delta f = \omega_c/\pi = 1/\pi$ yield center frequency NGD values of 2.07 s, 1.648 s, and 1.292 s, respectively. The corresponding time domain Gaussian pulse-peak advancement values in Fig. 17(b) are 2.254 s, 1.774 s, and 1.257 s, respectively, which are only 2.7%–8.9% of the frequency domain NGD values. The largest relative difference between observed NGD center frequency values and pulse-peak advancements in time is for the

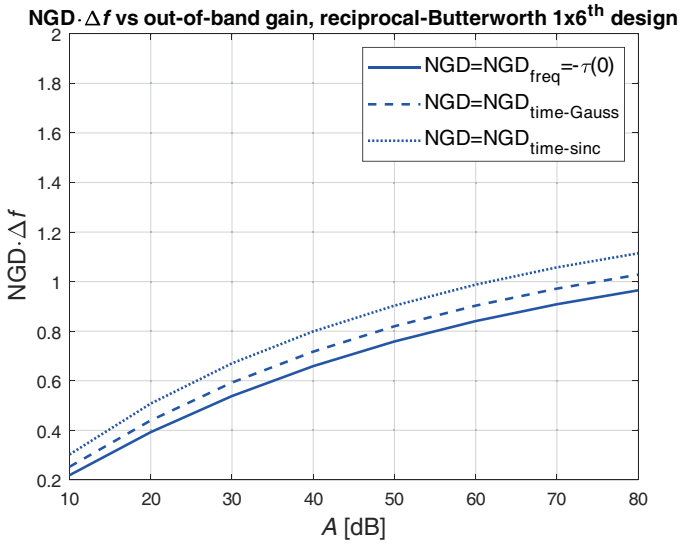

FIGURE 18. NGD-bandwidth product as a function of out-of-band gain for a 1×6^{th}-order capped reciprocal-Butterworth design with frequency domain, and corresponding time domain NGD for applied Gaussian and sinc pulses.

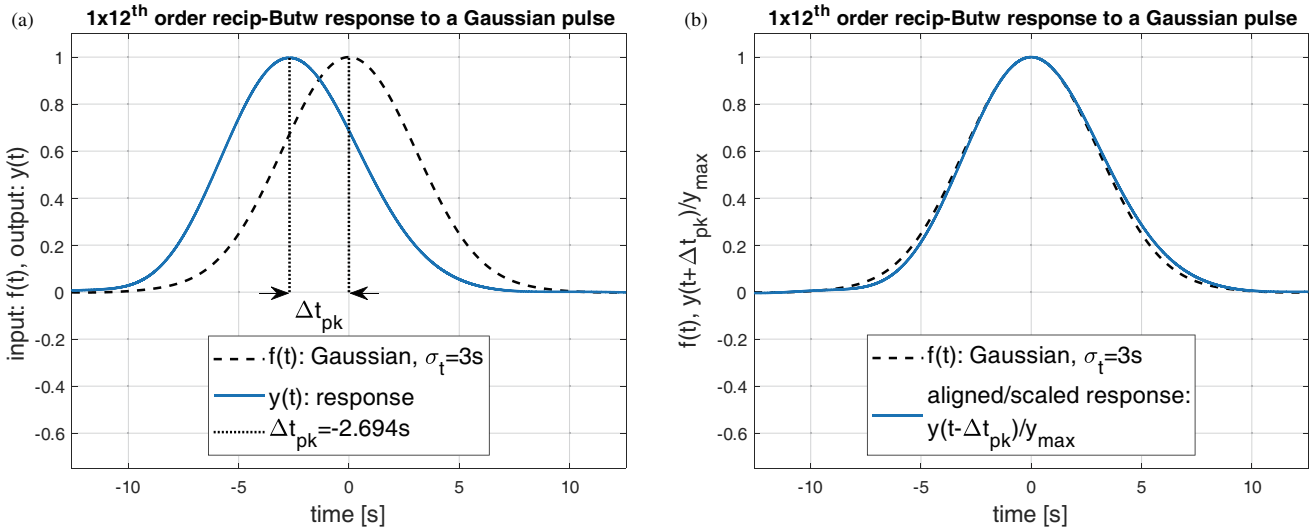

FIGURE 19. (a) Input Gaussian pulse with a frequency spectrum cut-off at $\omega_c = 1$, and the corresponding output waveform for a 1×12^{th}-order gain-compensated design. (b) The same comparison but with the output waveform shifted by Δt_{pk} and normalized by $|y(t)|_{\max}$.

1×6^{th} design in this example, since as evident from Fig. 2(b) higher order designs have a larger group delay variation. Conversely, higher order designs have less variation in their in-band frequency magnitude response (flatter response), as evident from Fig. 2(a) and Fig. 17(a), which then results in the amplitude of the time domain peak being closer to the input pulse amplitude, as evident from Fig. 17(b).

The group delay variation of higher order capped reciprocal-Butterworth designs is high around the band edges, as evident from Fig. 2(b), while the frequency spectrum power density of a Gaussian pulse is small close to band edges. Therefore, as seen in Fig. 18 when a Gaussian pulse is applied, the effects of in-band group delay variation are reduced, and the time domain observed peak advancement stays relatively close to the frequency domain NGD value at center frequency. As a contrasting example a sinc pulse, $\sin(\omega_c t)/(\omega_c t)$, has its power spectrum density constant within the entire bandwidth $(-\omega_c, \omega_c)$, and it is expected that it will exhibit a more prominent sensitivity to the group delay variation around the band edges. This is demonstrated in Fig. 18 where there is a larger difference between time and frequency NGD values for the sinc pulse.

Due to the inverse relationship between bandwidth and pulse duration, the NGD-bandwidth product metric in the frequency domain is proportional to the ratio of the pulse-peak advancement to any quantity representative of the pulse duration in the time domain. In the Gaussian pulse example, choosing its frequency spectrum standard deviation to be 1/6 of the 3 dB bandwidth of the medium, $\sigma_\omega = \Delta\omega/6$, the Gaussian pulse standard deviation in the time domain is $\sigma_t = 1/\sigma_\omega = 3/(\pi\Delta f)$. This yields a proportional relationship between the pulse-peak advancement to pulse standard deviation ratio in the time domain and the NGD-bandwidth product in the frequency domain,

$\text{NGD}/\sigma_t = (\pi/3) \cdot \text{NGD} \cdot \Delta f$. In the sinc pulse example, the duration between pulse peak and the first zero crossing is $t_0 = \pi/\omega_c$, yielding a proportional relationship between the pulse-peak advancement to duration t_0 ratio in the time domain and the NGD-bandwidth product in the frequency domain, $\text{NGD}/t_0 = \text{NGD} \cdot \Delta f$.

9. IN-BAND COMBINED MAGNITUDE/PHASE RESPONSE DISTORTION METRIC

The trade-off between the NGD-bandwidth product and the undesired out-of-band gain can be captured by a Figure of Merit (FOM), defined as the ratio of the two trade-off quantities [10]:

$$\text{FOM} = \frac{\text{NGD} \cdot \text{BW}}{A_{\text{dB}}}. \tag{34}$$

The out-of-band gain is proportional to the magnitude of time-domain transients when information carrying signals propagate through an NGD medium [8, 9]. Another NGD trade-off is distortion of the part of the signal which follows the settling of transients ("steady-state" part of the waveform). As discussed in Section 8, the transient response is associated with the out-of-band portion of the medium's frequency response, and conversely the "steady-state" part of the propagated waveform is associated with medium's in-band frequency response. Distortion of the "steady-state" part is due to in-band phase nonlinearity (non-constant group delay), as well as non-constant magnitude response within the specified (typically 3 dB) bandwidth. This in-band distortion is also applicable to continuous waveforms, which have no associated transients. Further, for applications where transients are not a concern, an alternative formulation of (34) can be applied where $1/A_{\text{dB}}$ is replaced by the center frequency magnitude response, $|H(j\omega_0)|$.

For a general time-domain input waveform $f(t)$, with its frequency spectrum given by $F(j\omega)$, an in-band combined magnitude/phase distortion metric for a baseband transfer function $H(j\omega)$ can be evaluated in a similar manner as that proposed in [13, 14], and as given in [10]:

$$D_{\textit{in-band}} = \sqrt{\frac{\int_0^{\omega_c} \left| F(j\omega) - e^{-j\omega\Delta t_{pk}} \cdot F(j\omega) \cdot H(j\omega) \cdot |f(t)|_{\max} / |y(t)|_{\max} \right|^2 d\omega}{\int_0^{\omega_c} |F(j\omega)|^2 \, d\omega}}. \tag{35}$$

Here Δt_{pk} is the resulting time-domain advancement of the waveform peak, and ω_c is the 3 dB cut-off, while $|f(t)|_{\max}$ and $|y(t)|_{\max}$ are the respective magnitudes of the input and output peaks. For NGD bandwidths and waveforms that are centered around a non-zero frequency, the baseband expression (35) is modified such that limits of both integrals span over the 3 dB bandwidth around the center frequency. Since linear scaling and time shift of a waveform do not contribute to distortion, the output spectrum in the numerator of expression (35), $F(j\omega) \cdot H(j\omega)$, is scaled and shifted to match the magnitude and position of the input waveform peak. In the distortion metric (35), the output spectrum scaling and shifting used is based on the exact observed time-domain output pulse peak magnitude and time-shift as done in [10], which are in general different from corresponding frequency domain parameters, as demonstrated in Figs. 17(b) and 18. In [13, 14], the output spectrum scaling and shifting are approximated by the center frequency magnitude and group delay response values, i.e., $|f(t)|_{\max}/|y(t)|_{\max} \approx 1/H(0)$ and $\Delta t_{pk} \approx -\tau(0)$, respectively. The distortion metric in expression (35) is more easily evaluated in the frequency domain since it involves finite integral bounds over the bandwidth. An equivalent evaluation in the time domain (yielding the same result) would involve infinite integrals of the input and output waveforms.

As an example, the distortion metric is examined for a Gaussian pulse input waveform with a frequency spectrum standard deviation equal to $1/6^{th}$ of the NGD 3 dB-bandwidth. This waveform is applied as an input to a 1×12^{th}-order design with a chosen ω_c =1 and $A = 40$ dB. Input and output waveforms are depicted in Fig. 19, and from expression (35) the distortion metric is $D_{\text{in-band-Gaussian}} = 0.0424$. As a comparison, for a well-known 1^{st}-order low-pass filter baseband design, $D_{\text{low-pass-Gaussian}} = 0.0411$. The center frequency NGD of this design is $-\tau(0) = 2.442$ s with an NGD-bandwidth product of 0.7772, as evaluated in Fig. 14. This is somewhat lower than the time domain advancement of the Gaussian pulse shown in Fig. 19, where $\Delta t_{pk} = 2.694$ s (congruent with Fig. 18 showing that the time-domain NGD is higher than the frequency domain one).

As a second example, a sinc function is applied as input to the same 1×12^{th}-order design with out-of-band gain $A = 40$ dB. The input and output waveforms depicted in Fig. 20(a) show a pulse-peak advancement of $\Delta t_{pk} = 3.094$ s (higher than the Gaussian peak advancement of 2.694 s, which is also congruent with Fig. 18). The distortion evaluated from (35) is $D_{\text{in-band-sinc}} = 0.2498$. Compared to the 1^{st}-order low-pass filter design value of $D_{\text{low-pass-sinc}} = 0.1093$, it suggests a significantly higher level of distortion for a sinc pulse applied to the 1×12^{th}-order NGD design than Gaussian pulse (Fig. 20(b) compared with Fig. 19(b)).

To keep the distortion metric given by (35) below a desired limit (for example below the 1^{st}-order low-pass filter distortion metric for the same applied waveform), an alternative approach would be to reduce the effective bandwidth of the input below the medium's 3 dB cut-off ω_c (i.e., a wider time domain pulse is applied that corresponds to the reduced bandwidth). Figure 21 shows the NGD-bandwidth product (using time domain NGD) as a function of out-of-band gain for the 1×12^{th}-order

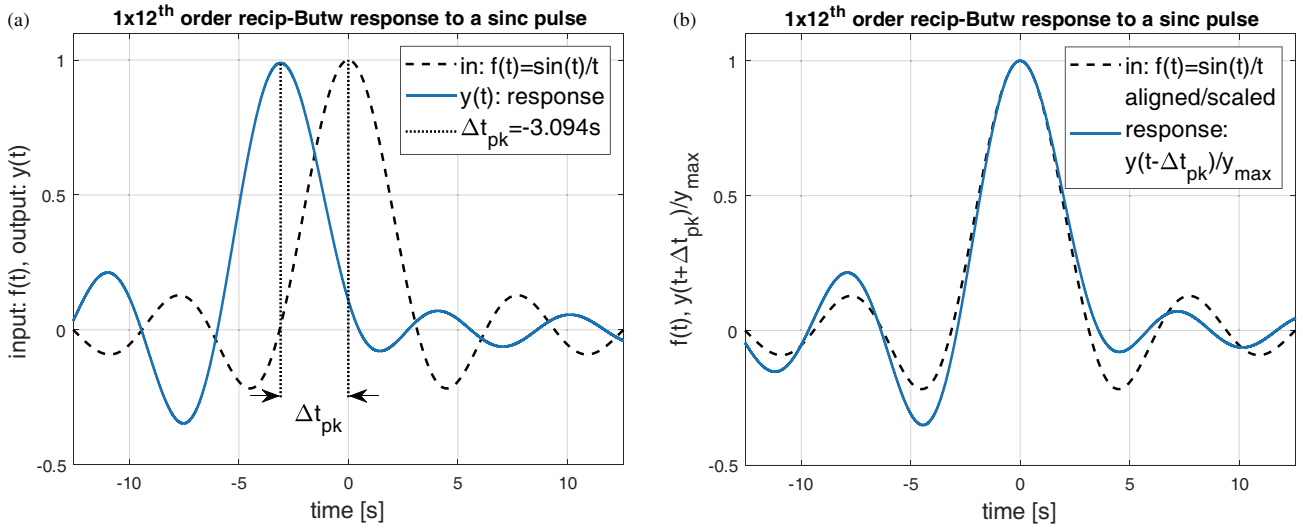

FIGURE 20. (a) Input sinc function with a corresponding constant frequency spectrum with cut-off at $\omega_c = 1$, and the corresponding output waveform for a 1×12^{th}-order gain-compensated design. b) The same comparison but with the output waveform shifted by Δt_{pk} and normalized by $|y(t)|_{\max}$.

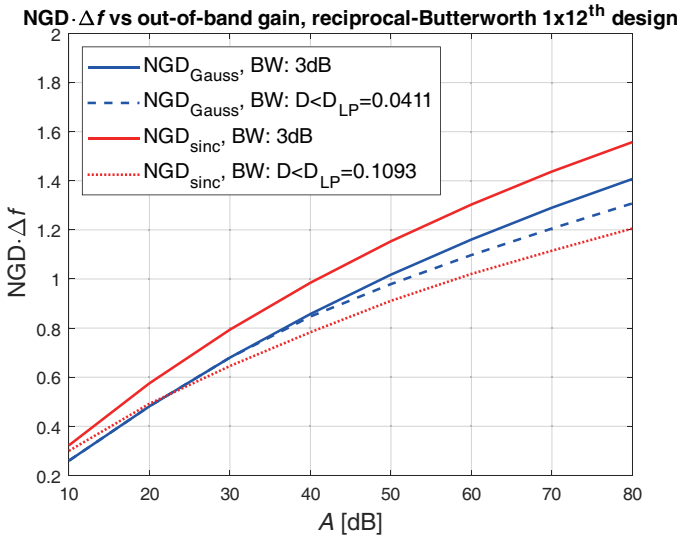

FIGURE 21. NGD-bandwidth product (using time domain NGD) for Gaussian and sinc inputs applied to the 12^{th}-order design with 3 dB bandwidth (solid curves) vs. reduced bandwidth yielding the same distortion metric as a 1^{st}-order low-pass filter ($D_{LP} = 0.0411, 0.1093$ for Gaussian and sinc inputs, respectively).

design, for a 3 dB bandwidth (solid curves) and for a reduced bandwidth needed to keep the distortion metric below that of a 1^{st}-order low-pass filter ($D = 0.0411$ for a Gaussian pulse, dashed curve, and $D = 0.1093$ for a sinc pulse, dotted curve). It can be noted from Fig. 21 that the NGD-bandwidth product is higher for the sinc input than the Gaussian input when distortion is ignored, i.e., input bandwidth kept at medium's 3 dB cut-off in both cases (solid curves). However, with the two inputs' respective bandwidths reduced to yield the distortion metric below that of a 1^{st}-order low-pass filter, NGD-bandwidth product for the Gaussian input (dashed curve) eventually surpasses the sinc input one (dotted curve), as the out-of-band gain increases. As discussed in Section 8, NGD-bandwidth product is proportional to an NGD to pulse-width ratio, where different options for representing a pulse-width (inversely proportional to bandwidth) yield different proportional factors. Further, it can be shown that a 1×12^{th}-order design achieves a higher NGD-bandwidth product (NGD taken as the time domain pulse-peak advancement) than a 2×6^{th}-order design for both waveform types, and both the 3 dB and distortion-considering reduced bandwidths. This is congruent with Fig. 15 trend with frequency domain NGD values (there, 1×6^{th}-order design outperforms 2×3^{rd}, 3×2^{nd}, and 6×1^{st}).

A complementary metric to the distortion metric (35) is a cross-correlation of input and output waveforms, as done in [28, 31]. It can be shown that it roughly relates to (35) as a square root of $1 - D^2$. Caution should be exercised, however, when interpreting seemingly high cross-correlation metric numbers (for example, a seemingly high cross-correlation

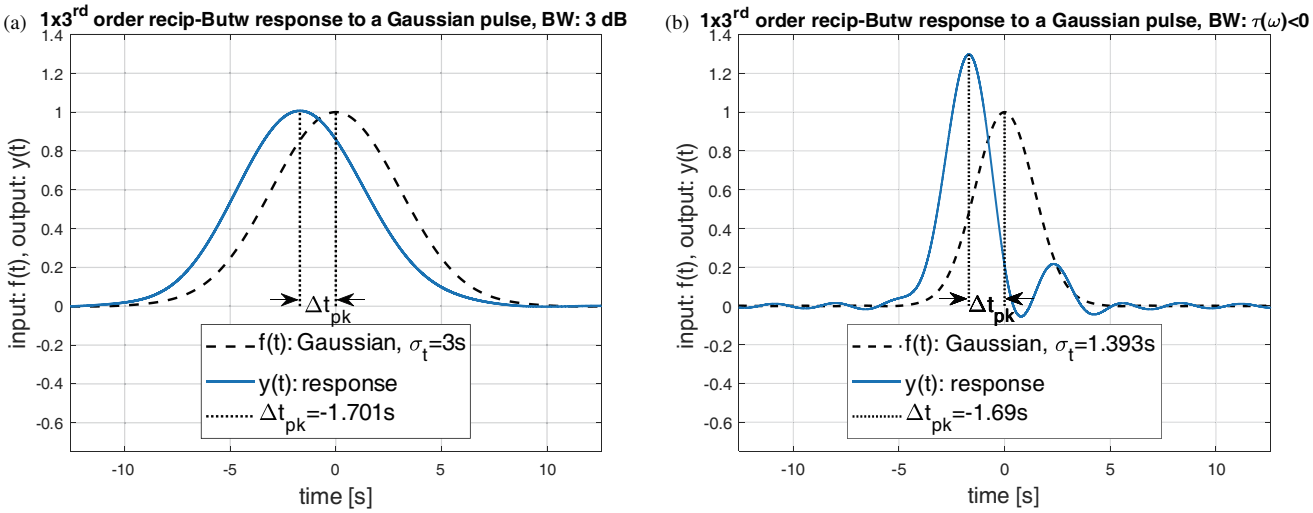

FIGURE 22. Capped reciprocal-Butterworth 1×3^{rd}-order gain-compensated design response to an input Gaussian pulse with its frequency spectrum a) within the 3 dB bandwidth of the design, and b) within the $\tau(\omega) < 0$ bandwidth (2.1544× wider, leading to a distortion metric 7.319× higher than that of a 1^{st}-order low-pass filter reference).

metric of 0.95 corresponds to a quite severe distortion metric of about 0.31).

It can be noted that imposing an in-band distortion limit on an NGD design assumes that one of the objectives is to maintain reasonable output waveform fidelity to the applied input waveform. However, in NGD design applications targeting group delay (and/or magnitude) response equalization of a preceding communication channel stage (for example, to mitigate positive group delay narrow-band spikes), the presented distortion limit can be either dropped or imposed on the overall design including the preceding stage(s) and the equalizing NGD design. For example, the use of an NGD circuit for equalizing both the magnitude and a group delay of a resonant system was demonstrated by Ravelo et al. [34, 35].

10. IMPLICATIONS OF USING THE ENTIRE BANDWIDTH WHERE GROUP DELAY IS NEGATIVE

In majority of the NGD circuit designs and applications presented in the literature, the NGD bandwidth that is reported is the entire frequency range where the group delay response is negative, $\tau(\omega) < 0$. Typically, this can be considerably wider than the 3 dB bandwidth, which is the criteria used in this paper (or lower, when distortion metric is above a prescribed level). It should be kept in mind that a $\tau(\omega) < 0$ defined bandwidth is likely to result in a high distortion metric for waveforms corresponding to that bandwidth. Group delay response zero-crossings of an N^{th}-order baseband design can be determined by equating to zero the sum of group delay expressions given by (4c) and/or 5(c), corresponding to all the 1^{st} and 2^{nd}-order factorized transfer functions, respectively, which comprise the overall N^{th}-order design. For a capped reciprocal-Butterworth design, while keeping in mind parameter relationships evident from (2a) and (2b) it can be shown that the group delay zero-crossings considered individually for all 1^{st} and 2^{nd}-order factorized functions are the same, $\omega_{\tau=0} = A^{1/(2N)}$ (and multiplied by the 3 dB bandwidth correction factor given by (6), $C_{\omega-3\,\mathrm{dB}}$). Therefore, the overall N^{th}-order design will also have the same group delay zero-crossings, $\omega_{\tau=0} = A^{1/(2N)} \cdot C_{\omega-3\,\mathrm{dB}}$, since it is a sum of individual terms that all have the same zero-crossings. Further, for the general capped reciprocal-Butterworth design proposed in this paper consisting of n cascaded stages of N^{th}-order and the overall out-of-band gain A_{dB}, the ratio of $\tau(\omega) < 0$ and 3 dB bandwidths, and the corresponding in-band magnitude variation within $\tau(\omega) < 0$ bandwidth, can be derived as:

$$\frac{\mathrm{BW}_{\tau<0}}{\mathrm{BW}_{3\,\mathrm{dB}}} = A^{1/(2nN)} \left(\frac{1 - \left(\frac{2}{A^2}\right)^{1/n}}{2^{1/n} - 1} \right)^{\frac{1}{2N}},$$

$$\Delta A_{\mathrm{dB,in-band},\tau<0} = \frac{A_{\mathrm{dB}}}{2}. \tag{36}$$

For example, applying (36) for a 1×3^{rd}-order design with 40 dB out-of-band gain ($n = 1$, $N = 3$, $A = 100$) yields a $\tau(\omega) < 0$ to 3 dB bandwidth ratio of 2.1544 (as corroborated in Fig. 2(b)). This yields a distortion metric from expression (35) of 0.3008 for a Gaussian waveform (7.319 times higher than distortion metric of a 1^{st}-order low-pass filter distortion, used a reference). Additionally, the in-band magnitude variation for $\tau(\omega) < 0$ is $A_{\mathrm{dB}}/2 = 20$ dB, as corroborated in Fig. 2(a). This leads to an unacceptable level of pulse distortion as demonstrated in Fig. 22(b). As another example, a 3×1^{st}-order design (compared to 1×3^{rd}-order design) has an even higher $\tau(\omega) < 0$ to 3 dB bandwidth ratio of 4.1004 according to (36), yielding a Gaussian waveform distortion metric of 0.4654 (11.324 times higher than 1^{st}-order low-pass filter reference). As evident from Fig. 2(b), lower order designs have a larger $\tau(\omega) < 0$ bandwidth, and therefore higher corresponding distortion.

Due to $\tau(\omega) < 0$ bandwidth having an $A_{\mathrm{dB}}/2$ relationship to the out-of-band gain, any design with an out-of-band gain larger

TABLE 1. NGD performance metrics for selected $n \times N^{\text{th}}$-order baseband topologies, with 3 dB bandwidth.

Number of stages/topology	Out-of-band gain, A [dB]	NGD-BW product, $-\tau(0) \cdot \Delta f_{3\text{dB}}$	FOM [1/dB]	$\Delta t_{\text{pk}} \cdot \Delta f_{3\text{dB}}$ (Gaussian)	Distortion: $D_{\text{in-band}}$ (Gaussian)
$1 \times 1^{\text{st}}$-order	40	0.3152	0.0079	0.2880	0.0432 ($1.05 \times D_{\text{1st-LP-filter}}$)
$1 \times 2^{\text{nd}}$-order	40	0.4052	0.0101	0.4368	0.0217 ($0.53 \times D_{\text{1st-LP-filter}}$)
$2 \times 1^{\text{st}}$-order	40	0.3714	0.0093	0.3544	0.0383 ($0.93 \times D_{\text{1st-LP-filter}}$)
$1 \times 3^{\text{rd}}$-order	40	0.4995	0.0125	0.5416	0.0227 ($0.55 \times D_{\text{1st-LP-filter}}$)
$3 \times 1^{\text{st}}$-order	40	0.3936	0.0100	0.3800	0.0369 ($0.90 \times D_{\text{1st-LP-filter}}$)
$1 \times 12^{\text{th}}$-order	40	0.7772	0.0194	0.8576	0.0424 ($1.03 \times D_{\text{1st-LP-filter}}$)
$2 \times 6^{\text{th}}$-order	40	0.7293	0.0182	0.8008	0.0377 ($0.92 \times D_{\text{1st-LP-filter}}$)

TABLE 2. NGD performance metrics for selected $n \times N^{\text{th}}$-order baseband topologies, with $\tau(\omega) < 0$ bandwidth.

Number of stages/topology	Out-of-band gain, A [dB]	NGD-BW product, $-\tau(0) \cdot \Delta f_{\tau<0}$	$\text{BW}_{\tau<0}/\text{BW}_{3\text{dB}}$	$\Delta t_{\text{pk}} \cdot \Delta f_{\tau<0}$ (Gaussian)	Distortion: $D_{\text{in-band}}$ (Gaussian)
$1 \times 1^{\text{st}}$-order	40	3.1513	9.999	0.8104	0.6288 ($15.3 \times D_{\text{1st-LP-filter}}$)
$1 \times 2^{\text{nd}}$-order	40	1.2812	3.162	1.0688	0.4640 ($11.3 \times D_{\text{1st-LP-filter}}$)
$2 \times 1^{\text{st}}$-order	40	1.8119	4.879	0.9760	0.5183 ($12.6 \times D_{\text{1st-LP-filter}}$)
$1 \times 3^{\text{rd}}$-order	40	1.0761	2.154	1.1592	0.3008 ($7.32 \times D_{\text{1st-LP-filter}}$)
$3 \times 1^{\text{st}}$-order	40	1.6141	4.100	1.0168	0.4654 ($11.3 \times D_{\text{1st-LP-filter}}$)
$1 \times 12^{\text{th}}$-order	40	0.9416	1.212	1.1720	0.1439 ($3.50 \times D_{\text{1st-LP-filter}}$)
$2 \times 6^{\text{th}}$-order	40	0.9498	1.302	1.1952	0.1520 ($3.70 \times D_{\text{1st-LP-filter}}$)

than 6 dB will have in-band variation of more than 3 dB, and potentially cause high levels of distortion. For NGD designs different from ones presented in this paper, the exact relationship may be different from $A_{\text{dB}}/2$, but the in-band magnitude variation value should be noted for the $\tau(\omega) < 0$ bandwidth, and if larger than 3 dB the entire $\tau(\omega) < 0$ bandwidth may not be practically useful when distortion is considered. Further, even the 3 dB bandwidth may be too large if a specified level of distortion is exceeded. As demonstrated in this paper, an NGD design should be checked for distortion for the time domain waveforms of interest.

11. CONCLUSION

In this paper, an NGD filter prototype baseband design based on capped reciprocal N^{th}-order Butterworth low-pass filter transfer function is introduced. The baseband design can be translated to an NGD band-stop filter with finite attenuation at a desired center frequency. It is shown that the upshifted center frequency design can be exactly implemented with a Sallen-Key topology. Further, a ladder network of series RLC resonators connected in shunt, and parallel resonators connected in series, is shown to be able to approximately model the upshifted design, without the use of op-amps. The process of calculating the component values of both Sallen-Key and all-passive ladder designs is outlined in detail.

The prototype design achieves an NGD-bandwidth product that in the upper asymptotic limit as the design order approaches infinity is a linear function of out-of-band gain in decibels. Further, for a cascaded N^{th}-order design, the NGD-bandwidth product upper asymptotic limit (distributed design, number of stages approaches infinity, but the overall out-of-band gain stays the same) is a function of out-of-band gain in decibels raised to the power $1 - 1/(2N)$. Out-of-band gain, a trade-off quantity accompanying NGD designs, was shown to be proportional to transient magnitudes of the proposed design for information carrying signals with finite turn-on/off instants in time, as it was for previously reported designs [8–10].

An in-band distortion metric based on the approach in [13, 14] and modified as in [10] is applied to the proposed design and given time-domain input waveforms. Different waveforms result in different distortion metrics. A sinc input function for example is shown to yield a higher distortion metric than a Gaussian pulse, since it has a constant frequency spectrum over the entire bandwidth and therefore has equal contributions in magnitude and phase distortion across the bandwidth. Table 1 shows a performance comparison of selected proposed NGD designs with a given order and number of cascaded stages, in terms of their achieved NGD in the frequency domain as well as in the time domain for a Gaussian input waveform. The associated Figure-of-Merit (FOM) and distortion metric is also shown.

It was demonstrated that selecting a bandwidth which spans over the entire frequency range where the group delay response is negative, $\tau(\omega) < 0$, results in an in-band magnitude response variation of half that of the out-of-band decibel value, $A_{\text{dB}}/2$, and is likely to result in an unacceptably high distortion. Table 2 summarizes metrics for the same examples from Table 1, when a larger, $\tau(\omega) < 0$ bandwidth is used instead of the 3 dB bandwidth. A 1^{st}-order low-pass filter is used as a reference for comparing the distortion performance. It is prudent to check the in-band magnitude response variation for a specified bandwidth of an NGD design and be cautious of any in-band variations over 3 dB. In addition to the out-of-band gain, a commonly stated trade-off for NGD designs, an in-band combined magnitude-phase distortion metric over a specified bandwidth should also be considered to ensure an acceptable level of waveform distortion.

REFERENCES

[1] Brillouin, L., *Wave Propagation and Group Velocity*, Academic Press, 2013.

[2] Mojahedi, M., K. J. Malloy, G. V. Eleftheriades, J. Woodley, and R. Y. Chiao, "Abnormal wave propagation in passive media," *IEEE Journal of Selected Topics in Quantum Electronics*, Vol. 9, No. 1, 30–39, 2003.

[3] Stenner, M. D., D. J. Gauthier, and M. A. Neifeld, "Fast causal information transmission in a medium with a slow group velocity," *Physical Review Letters*, Vol. 94, No. 5, 053902, 2005.

[4] Mojahedi, M., E. Schamiloglu, F. Hegeler, and K. J. Malloy, "Time-domain detection of superluminal group velocity for single microwave pulses," *Physical Review E*, Vol. 62, No. 4, 5758, 2000.

[5] Wang, Y., Y. Zhang, L. He, F. Liu, H. Li, and H. Chen, "Direct observation of negative phase velocity and positive group velocity in time domain for composite right/left-handed transmission lines," *Journal of Applied Physics*, Vol. 100, No. 11, 113503, 2006.

[6] Ibraheem, I. A., J. Schoebel, and M. Koch, "Group delay characteristics in coplanar waveguide left-handed media," *Journal of Applied Physics*, Vol. 103, No. 2, 2008.

[7] Bolda, E. L., R. Y. Chiao, and J. C. Garrison, "Two theorems for the group velocity in dispersive media," *Physical Review A*, Vol. 48, No. 5, 3890, Nov. 1993.

[8] Kandic, M. and G. E. Bridges, "Asymptotic limits of negative group delay in active resonator-based distributed circuits," *IEEE Transactions on Circuits and Systems I: Regular Papers*, Vol. 58, No. 8, 1727–1735, Aug. 2011.

[9] Kandic, M. and G. E. Bridges, "Limits of negative group delay phenomenon in linear causal media," *Progress In Electromagnetics Research*, Vol. 134, 227–246, 2013.

[10] Kandic, M. and G. E. Bridges, "Negative group delay prototype filter based on cascaded second order stages implemented with Sallen-Key topology," *Progress In Electromagnetics Research B*, Vol. 94, 1–18, 2021.

[11] Solli, D., R. Y. Chiao, and J. M. Hickmann, "Superluminal effects and negative group delays in electronics, and their applications," *Physical Review E*, Vol. 66, No. 5, 056601, 2002.

[12] Dorrah, A. H. and M. Mojahedi, "Nonanalytic pulse discontinuities as carriers of information," *Physical Review A*, Vol. 93, No. 1, 013823, 2016.

[13] Macke, B., B. Ségard, and F. Wielonsky, "Optimal superluminal systems," *Physical Review E*, Vol. 72, No. 3, 035601(R), Sep. 2005.

[14] Macke, B. and B. Segard, "Propagation of light-pulses at a negative group-velocity," *The European Physical Journal D — Atomic, Molecular, Optical and Plasma Physics*, Vol. 23, 125–141, Apr. 2003.

[15] Lucyszyn, S., I. D. Robertson, and A. H. Aghvami, "Negative group delay synthesiser," *Electronics Letters*, Vol. 29, No. 9, 798–800, Apr. 1993.

[16] Nakanishi, T., K. Sugiyama, and M. Kitano, "Demonstration of negative group delays in a simple electronic circuit," *American Journal of Physics*, Vol. 70, No. 11, 1117–1121, Nov. 2002.

[17] Kitano, M., T. Nakanishi, and K. Sugiyama, "Negative group delay and superluminal propagation: An electronic circuit approach," *IEEE Journal of Selected Topics in Quantum Electronics*, Vol. 9, No. 1, 43–51, Feb. 2003.

[18] Siddiqui, O. F., M. Mojahedi, and G. V. Eleftheriades, "Periodically loaded transmission line with effective negative refractive index and negative group velocity," *IEEE Transactions on Antennas and Propagation*, Vol. 51, No. 10, 2619–2625, Oct. 2003.

[19] Ravelo, B., A. PÉrennec, M. L. Roy, and Y. G. Boucher, "Active microwave circuit with negative group delay," *IEEE Microwave and Wireless Components Letters*, Vol. 17, No. 12, 861–863, Dec. 2007.

[20] Choi, H., Y. Jeong, C. D. Kim, and J. S. Kenney, "Bandwidth enhancement of an analog feedback amplifier by employing a negative group delay circuit," *Progress In Electromagnetics Research*, Vol. 105, 253–272, 2010.

[21] Mirzaei, H. and G. V. Eleftheriades, "Realizing non-foster reactive elements using negative-group-delay networks," *IEEE Transactions on Microwave Theory and Techniques*, Vol. 61, No. 12, 4322–4332, Dec. 2013.

[22] Chaudhary, G., Y. Jeong, and J. Lim, "Microstrip line negative group delay filters for microwave circuits," *IEEE Transactions on Microwave Theory and Techniques*, Vol. 62, No. 2, 234–243, Feb. 2014.

[23] Wu, C.-T. M. and T. Itoh, "Maximally flat negative group-delay circuit: A microwave transversal filter approach," *IEEE Transactions on Microwave Theory and Techniques*, Vol. 62, No. 6, 1330–1342, Jun. 2014.

[24] Chaudhary, G. and Y. Jeong, "Transmission-type negative group delay networks using coupled line doublet structure," *IET Microwaves, Antennas & Propagation*, Vol. 9, No. 8, 748–754, 2015.

[25] Chaudhary, G. and Y. Jeong, "Negative group delay phenomenon analysis using finite unloaded quality factor resonators," *Progress In Electromagnetics Research*, Vol. 156, 55–62, 2016.

[26] Wu, Y., H. Wang, Z. Zhuang, Y. Liu, Q. Xue, and A. A. Kishk, "A novel arbitrary terminated unequal coupler with bandwidth-enhanced positive and negative group delay characteristics," *IEEE Transactions on Microwave Theory and Techniques*, Vol. 66, No. 5, 2170–2184, 2018.

[27] Wan, F., N. Li, B. Ravelo, and J. Ge, "O = O shape low-loss negative group delay microstrip circuit," *IEEE Transactions on Circuits and Systems II: Express Briefs*, Vol. 67, No. 10, 1795–1799, Oct. 2020.

[28] Ravelo, B., F. Wan, and J. Ge, "Anticipating actuator arbitrary action with a low-pass negative group delay function," *IEEE Transactions on Industrial Electronics*, Vol. 68, No. 1, 694–702, Jan. 2021.

[29] Wang, Z., S. Zhao, H. Liu, and S. Fang, "A compact dual-band differential negative group delay circuit with wideband common mode suppression," *IEEE Journal of Microwaves*, Vol. 2, No. 4, 720–725, Oct. 2022.

[30] Nair, R. G. and S. Natarajamani, "Design theory of compact power divider with reconfigurable power division and negative group delay characteristics," *Scientific Reports*, Vol. 13, No. 1, 7222, May 2023.

[31] Ravelo, B., H. Bilal, S. Rakotonandrasana, M. Guerin, F. Haddad, S. Ngoho, and W. Rahajandraibe, "Transient characterization of new low-pass negative group delay RC-network," *IEEE Transactions on Circuits and Systems II: Express Briefs*, Vol. 71, No. 1, 126–130, Jan. 2024.

[32] United States Patent Office (USPTO) application number: 18/491922.

[33] Ravelo, B., "Similitude between the NGD function and filter gain behaviours," *International Journal of Circuit Theory and Applications*, Vol. 42, No. 10, 1016–1032, 2014.

[34] Ravelo, B., F. Wan, J. Nebhen, W. Rahajandraibe, and S. Lalléchère, "Resonance effect reduction with bandpass negative group delay fully passive function," *IEEE Transactions on Circuits and Systems II: Express Briefs*, Vol. 68, No. 7, 2364–2368, Jul. 2021.

[35] Ravelo, B., S. Lalléchère, W. Rahajandraibe, and F. Wan, "Electromagnetic cavity resonance equalization with bandpass negative group delay," *IEEE Transactions on Electromagnetic Compatibility*, Vol. 63, No. 4, 1248–1257, Aug. 2021.